Nanoscale

Accepted Manuscript

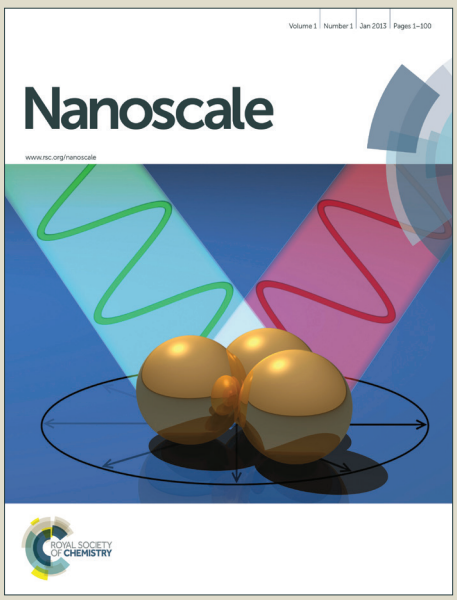

ROYAL SOCIETY OF CHEMISTRY

www.rsc.org/nanoscale

Cite this: DOI: 10.1039/c0xx00000x

www.rsc.org/xxxxxx

Paper

Solution combustion synthesis of metal oxide nanomaterials for energy storage and conversion†

Fa-tang Li,[§ab] Jingrun Ran,[§b] Mietek Jaroniec[c] and Shi Zhang Qiao*[b]

Received (in XXX, XXX) Xth XXXXXXXXX 2015, Accepted Xth XXXXXXXXX 20XX

DOI: 10.1039/b000000x

Design and synthesis of metal oxide nanomaterials is one of the key steps for achieving the highly efficient energy conversion and storage on industrial scale. Solution combustion synthesis (SCS) is a time- and energy-saving method as compared with other routes, especially for the preparation of complex oxides, which can be easily adapted for scale-up applications. This review summarizes the synthesis of various metal oxide nanomaterials and their applications for energy conversion and storage, including lithium-ion batteries, supercapacitors, hydrogen and methane production, fuel cells and solar cells. Especially, some novel concepts such as reverse support combustion, self-combustion of ionic liquids, and creation of oxygen vacancies are presented. SCS has some unique advantages such as the capability for in-situ doping of oxides and construction of heterojunctions. The well-developed porosity and large specific surface area caused by gas evolution during combustion process endow the resulting materials with exceptional properties. The relationship between the structural properties of the metal oxides studied and their performance is discussed. Finally, conclusions and perspectives are briefly presented.

1. Introduction

With continuously rapid consumption of fossil fuels, the conversion of solar energy to the other consumable forms of energy as well as energy storage have become important issues of the current and future research. To meet the world's fast-growing energy demand, the development of inexpensive materials for energy conversion and storage is a very important task for large-scale industrial applications. Generally, most of these compounds are metal oxide nanomaterials because of their small size, surface and quantum effects, resulting in the unique properties. There are many strategies for the synthesis of metal oxide nanomaterials; namely, sol–gel, chemical co-precipitation, chemical vapor deposition, mechanical alloying, solvothermal synthesis, microwave heating, and reverse micelle synthesis.[1-3] However, many of these methods require long reaction time, high external temperature, or special instrumentation. Meanwhile, with continuously increasing deterioration of environment caused by emissions of various pollutants and the inevitable depletion of fossil energy, the green and economic production of materials for reducing pollution and saving energy becomes more and more important issue.

In 1967 Merzhano et al. presented the concept of self-spreading high-temperature synthesis[4] (SHS, also known as combustion synthesis) based on their extensive studies of combustion of condensed substances. This method takes advantage of exothermicity of the self-sustaining chemical reaction itself to drive the reaction.[5] However, for this type of reaction involving solid reagents under combustion conditions,[6] the major drawbacks are difficulties in controlling SHS process and large size of particles. As a result, this method is not suitable for the preparation of complex oxides.[7] Subsequently, Patil et al. further developed this method, known as solution combustion synthesis (SCS), by combining it with wet chemistry.[8]

Solution combustion synthesis employs metal salts, including nitrates, sulfates and carbonates, as oxidants, and fuels as reducing reagents, such as urea, glycine, sucrose, starch, based on the exothermicity of the redox reaction. The released heat of the combustion reaction fulfils the energy requirement for the formation of oxides, resulting in some cases in temperatures that exceed 3000 °C.[9] The most obvious advantage of SCS is its time- and energy-efficiency. Once the mixture of reagents is ignited, the high self-generated energy can convert precursors into the corresponding oxides without requirement of an additional external energy input. Hence, the products are formed in several minutes. Fig. 1 shows a series of pictures illustrating the formation process.[10]

In contrast, other synthesis based on metal hydroxides and/or alkoxides conversion is endothermic, demanding continuous external energy input.[11] Moreover, porous materials have been extensively used for energy storage, catalysis, sensing, adsorption and separation[12] because of their large surface areas available for reactions, interfacial transport, and/or dispersion of active sites.[13] Unlike hydrothermal,[14] electrodeposition,[15] chemical vapour deposition (CVD),[16] and atomic layer deposition (ALD)[17] methods that employ soft or hard templates and require special advanced instruments, SCS can easily afford porous materials due to their inherent characteristics.

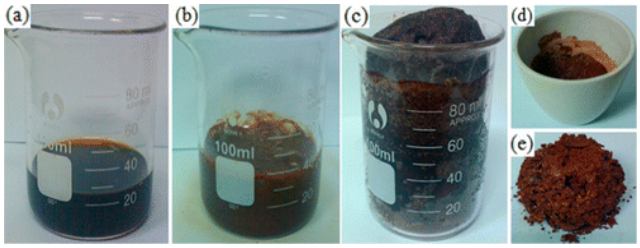

Fig. 1. Series of pictures illustrating the different preparation stages: (a) sol solution; (b) viscous gel; (c) dried gel; (d) as-burned product; (e) calcined product (if post-treatment is needed). Reproduced with permission from ref 10 Copyright © 2012, American Chemical Society.

Besides two most obvious advantages of the time/energy-efficiency and well-developed porosity, there are other advantages of SCS: (i) simplicity and low cost of instrumentation,[18] and the easiness of scaling-up SCS; (ii) possibility of obtaining products with diverse functionality and structures such as metallics, intermetallics, metal-matrix composites, cermets, solid solutions, carbides, nitrides, borides, ceramics, and oxides;[19] (iii) possibility of synthesizing ternary or quaternary oxides with high purity, which is very difficult to achieve otherwise because of the complex structures and low rate of solid state reactions; (iv) opportunity of achieving novel performance because some metastable phases can be formed in a short time;[20] and (v) in the case of heterogeneous photocatalysts, the materials with high active surface area can be prepared via SCS, which is beneficial for the transfer and separation of charge carriers.[21] A homogeneous mixed solution and high reaction temperature ensure the formation of complex oxides. Furthermore, environmentally benign raw materials can be used in this method (unlike, for example, in chemical vapor deposition or molecular beam epitaxy).

This review presents the recent achievements in the SCS processing of various metal oxide nanomaterials and their applications in energy conversion and storage devices, including lithium-ion batteries, supercapacitors, hydrogen and methane production, fuel cells and solar cells. Also, a newly developed SCS method, involving self-combustion of ionic liquids, is briefly discussed. A special emphasis is placed on the relationship between the structure of metal oxide nanomaterials and their performance, and on the formation of surface oxygen vacancies in these materials.

2. Fundamentals of solution combustion synthesis

Reaction temperature is a crucial parameter in the synthesis of materials. The combustion temperature can be approximately estimated by the following equation:[22]

$$T_c = T_0 + (\Delta H_r^0 - \Delta H_p^0)/C_p \quad (1)$$

where T_0 denotes the room temperature, $\triangle H_r^0$ and $\triangle H_p^0$ are the enthalpies of formation of the reactants and products, respectively, and C_p is the heat capacity of the products at a constant pressure. Nevertheless, the authentic temperature of a combustion reaction is generally much lower than the calculated theoretical T_c as a result of various factors including the heat evolution of a larger amount of gas, incomplete combustion of fuels, and loss of heat by radiation.[23–25] It should be noted that high temperature can result in the shrinkage of pores, which results in the smaller pore volumes, and lower specific surface areas of the products.

Among various metal salts, hydrated nitrates are preferred as metal precursors, because of not only the efficient oxidizing power of NO_3^- groups, but also their lower decomposition temperature and good solubility in water.[10] Furthermore, urea ($CO(NH_2)_2$) and glycine (NH_2CH_2COOH) are the most common fuels used due to their low cost, good availability, high exothermicity, as well as their high coordination ability toward nitrates. For the purpose of illustration, Fig. 2 shows the coordination structure for $Fe(NO_3)_3/Al(NO_3)_3$-urea system. It is suggested that urea molecules are situated in the second coordination sphere near the carbon atom, while nitrate radical anions are in the outer coordination sphere. This structure facilities the stabilization of reactive nitrates at an ambient atmosphere.[10] Varma et al.[26] found that the activity of $-NH_2$ is higher than that of the -OH group, which in turn is more active than -COOH based on the studies of iron nitrate with three model fuels. Urea containing two amino groups located at both ends of its chemical structure,[27] and glycine with an amino group located at one end of the chain and a carboxylic acid group at the other end,[25] are attractive fuels. The presence of COOH group in glycine, easily complexing metal ions, explains why it is a more reactive fuel than citric acid ($HOC(CH_2)_2(COOH)_3$), which possesses only -OH and -COOH.[28]

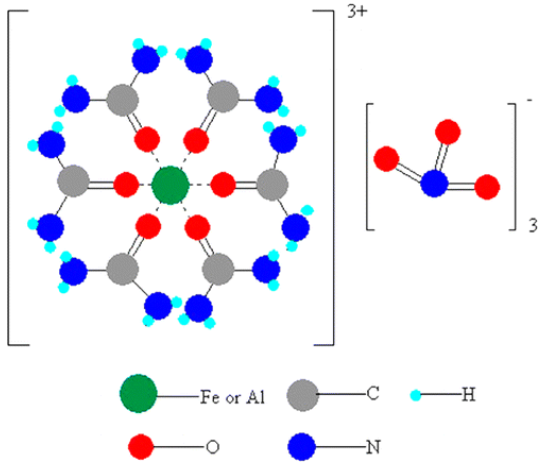

Fig. 2. Proposed coordination structure of Fe (Al)-urea-nitrate complex. Reproduced with permission from ref 10 Copyright © 2012, American Chemical Society.

Apart from the fuel types, the fuel amount is also one of the key parameters influencing the morphology, particle size, and specific surface area of the product. The fuel/oxidizer ratio, φ, is defined by the following equation proposed by Jain et al.[29] Herein, the reaction between urea ($CO(NH_2)_2$) and $M(NO_3)_v$ is taken as an example to illustrate calculations and N_2 is considered as the product of N element in the reaction.

$$\varphi = \frac{total\ valency\ of\ fuel}{total\ valency\ of\ oxidizer} = -\frac{n(4_{(C)} \times 1 - 2_{(O)} + 0_{(N)} \times 2 + 1_{(H)} \times 4)}{\nu_{(M)} + \nu(0_{(N)} - 2_{(O)} \times 3)} \quad (2)$$

where n is the number of moles of urea and ν is the oxidation

state of metal element M. Accordingly, the stoichiometric equilibrium combustion reaction can be expressed by the following equation:[30]

$$M(NO_3)_\nu + (\frac{5}{6}\nu\varphi)CO(NH_2)_2 + \nu\frac{15}{6}(\varphi-1)O_2 \rightarrow$$
$$MO_{\nu/2} + (\frac{5}{6}\nu\varphi)CO_2(g) + (\frac{5}{3}\nu\varphi)H_2O(g) + \nu(\frac{3+5\varphi}{6})N_2(g) \quad (3)$$

The mixture is stoichiometric when φ=1, fuel lean when φ>1 and fuel rich when φ<1. Equation (3) indicates that an addition of fuel (higher φ) into the system requires more oxygen. When at ambient atmosphere the oxygen supply is insufficient for combustion, the reaction is incomplete, which results in generating carbonaceous products. On the other hand, when the amount of fuel is small, the combustion temperature is low. Hence, the fuel amount is an important factor, which can be adjusted for controlling the degree of crystallinity and physical properties of the resulting materials.

Also, Eq. 3 shows that a large amount of gaseous products can be generated in the SCS process. For instance, the reaction of $Zn(NO_3)_2$ and urea with φ=1 releases nearly 7.7 moles of gas per mole of ZnO.[11] The released gas will produce a large number of pores in the oxide and inhibit their agglomeration, leading to a large specific surface area of the resulting material. On the other hand, the gas amount is also related to the φ value, as shown in Eq. (2). In general, higher φ value means larger amount of gaseous products and high combustion temperature. A large volume of the released gases leads to larger porosity and higher surface area, while higher combustion temperature enhances crystallinity and may reduce the surface area. Thus, the surface area represents a balance of two competing factors, the amount of gaseous products and the combustion temperature. It should be also mentioned that very high φ value (excessive amount of fuel) results in the lower combustion temperature and smaller crystallinity of the products because of the uncompleted combustion caused by insufficient amount of oxygen in the atmosphere.[31]

3. Synthesis of binary metal oxide nanomaterials

3.1 Pristine metal oxide nanomaterials

Simple binary metal oxides including TiO_2, ZnO, Fe_2O_3, etc. are the often used energy materials due to their low cost, earth-abundant availability, and high-efficiency. There is a great interest in developing a large-scale, inexpensive and facile SCS of these oxides instead of other high-cost methods.

In 1993, Patil's group reported for the first time the combustion synthesis of anatase TiO_2 and ZrO_2 via the exothermic decomposition of the coordination precursors of MO $(N_2H_3COO)_2 \cdot 2H_2O$ (M=Ti, Zr).[32] The $MO(N_2H_3COO)_2 \cdot 2H_2O$ (hydrazine carboxylates) were formed by reacting aqueous solutions of titanium and zirconium oxychlorides ($MOCl_2$) with solution of N_2H_3COOH in $N_2H_4 \cdot H_2O$ ($N_2H_5COON_2H_3$). Since $MOCl_2$ aqueous solutions are not commonly used reagents, titanyl nitrate obtained by hydrolysis of titanium isopropoxide has been often employed as precursor for the synthesis of TiO_2.[33-35] Fe_2O_3 is a typical semiconductor with narrow band gap (ca. 2.0-2.2 eV), which responds to visible light and can be used as an effective photocatalyst. Patil *et al.* also reported for the first time the combustion synthesis of γ-Fe_2O_3 using malonic acid dihydrazide ($C_3H_8N_4O_2$) as a fuel.[36] Another important member in iron oxides family, Fe_3O_4, is formed in the absence of air to avoid the oxidation of Fe^{2+} in Fe_3O_4 to Fe^{3+}. Mukasyan's group[37] and Deshpande et al.[38] reported the preparation of Fe_3O_4 powders with specific surface area of 50 m^2/g in argon (oxygen-free) atmosphere. On the other hand, Toniolo et al.[27] reported that the combustion product of iron nitrate-urea, which is a mixture of α-Fe_2O_3 and Fe_3O_4. Ianos et al.[39] verified the influence of air on the formation of iron oxides. They conducted a series of experiments in the absence and presence of air using the same fuels, respectively. The resulting products synthesized in air were mixtures of α- and γ-Fe_2O_3, whereas single Fe_3O_4 was obtained in the absence of air. Furthermore, the phase composition of the product was shown to be less affected by the fuel used, such as sucrose, citric acid, or glucose. On the contrary, Varma's group[28] found that the resulting products were affected not only by atmosphere, but also by the fuel used.

The search for economically feasible routes for the synthesis of metal oxides is of great importance for their potential industrial applications. Al_2O_3, an "earth abundant" and inexpensive material, has been widely used as a catalyst and catalyst's support.[40–42] Recently, our group has found that the partially amorphous Al_2O_3 obtained by combustion method showed photocatalytic activity under ultraviolet (UV) light[43] owing to its shorter Al-O bond length,[44] which makes it a potential energy material. The ratio of amorphous and crystalline phases in this material can be controlled by adjusting the fuel amount. Zhuravlev et al.[25] studied the influence of various fuels on the morphology of Al_2O_3. They found that the agglomerates of Al_2O_3 particles obtained in the presence of glycine have a friable structure; while Al_2O_3 aggregates obtained in the presence of urea are denser, larger and more durable without visible cellular structure.

Other energy materials including WO_3,[45,46] ZnO,[47,48] Co_3O_4,[49-51] SnO_2,[52] and ZrO_2,[53] have been also prepared via SCS, showing an extensive applicability of this route for the preparation of binary metal oxides.

On the other hand, it is well known that the morphology plays an important role in the performance of materials. There are several reports on the preparation of nanomaterials with special morphology via SCS. For instance, Kanatzidis et al.[11] fabricated diverse electronic metal oxide films (In_2O_3, and Zn–Sn–O, In–Zn–O, In-Sn-O solid solutions) by integrating combustion processing with solution deposition of oxide-based macroelectronics (see Fig. 3).

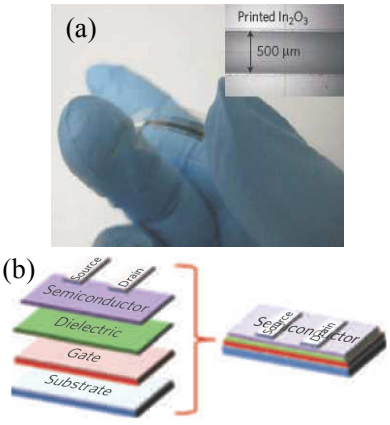

Fig. 3. (a) Optical image of a flexible combustion-processed In_2O_3 device on Ar (30 nm Al gate electrode/41 nm α-alumina dielectric, with 30 nm Al source and drain electrodes) and optical image of an inkjet printed In_2O_3 line on n++Si/41 nm α-alumina (inset). (b) The structure of a top-contact bottom-gate thin-film transistor. Reproduced with permission from ref 11 Copyright © 2011, Nature Publishing Group.

Nanorod-type structures have received a considerable attention. Nagabhushana and Chandrappa[54] reported the combustion synthesis of monoclinic VO_2 nanorods using solutions of ammonium metavanadate (NH_4VO_3) and DL-malic acid ($C_4H_6O_5$) as illustrated in Fig. 4. Kale et al.[55] employed glycine and ammonium nitrate as fuels to prepare nanosized necked-type structures α-Fe_2O_3 and γ-Fe_2O_3.

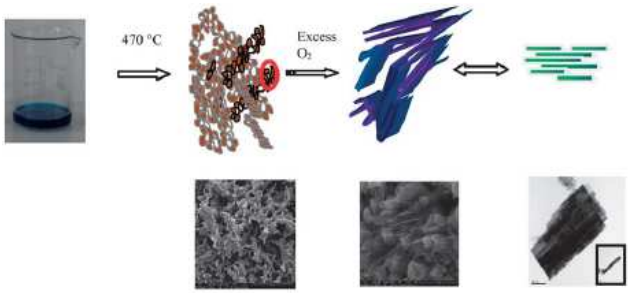

Fig. 4. Schematic illustration of the evolution of a VO_2 nanorod-like array. Reproduced with permission from ref 54 Copyright © 2013, Royal Society of Chemistry.

3.2 Defective metal oxide nanomaterials

3.2.1 Doping with nonmetal ions from fuels

Since traditional metal oxides with large band gaps, e.g., TiO_2 and ZnO, are inactive under visible-light irradiation,[56–58] a proper modification or doping with non-metals or metal ions, co-doping and noble metal deposition to produce defects have been explored to induce their visible-light activity.[58,59]

Ever since the pioneering work by Asahi et al.[60] showing that nitrogen-doped TiO_2 films and powders exhibit a prolonged light absorbance up to 500 nm and are effective in the degradation of methylene blue and gaseous acetaldehyde, doping of metal oxides with various nonmetal ions has been used to enhance their visible-light absorption and quantum yield. Various methods have been explored to dope TiO_2 with nonmetal ions (such as C, N, F, B, S, etc.). It was shown that the absorption spectra of TiO_2 doped with non-metal species are red-shifted to longer wavelengths, and exhibit higher photocatalytic activities as compared to that of pristine TiO_2, especially in the visible-light region.[61–66]

Although Asahi et al.[60] suggested that the visible light activity of N-doped TiO_2 is achieved due to the band-gap narrowing driven by mixing N 2*p* states with O 2*p* states, Lee and coworkers[67] concluded on the basis of the first-principles density-functional calculations that the absorption of visible light by N- or C-doped TiO_2 is due to the isolated N(C) 2*p* states above the valence-band maximum of TiO_2 rather than due to a band-gap narrowing. Based on the XPS spectra, Chen and co-workers[68] reported additional electronic states for C- and N-doped TiO_2 nanomaterials, which can explain the red-shifted absorption edge of these photocatalysts and their lowered oxidation potentials. However, Varley et al.[69] reported that N atom on the substitutional O sites (N_O) is the source of visible-light absorption through the photo-excitation of a localized electron from N_O to the extended conduction-band state. They pointed out that the substitutional N_O is a deep acceptor that gives rise to the sub-bandgap impurity-to-band transitions in the visible light range and the sub-bandgap absorption is unambiguously attributed to the substitutional N, and not to the interstitial N. Although the explanations of the role of N or C doped in TiO_2 are different, it is obvious that the N/C element doping with appropriate amount has positive effect on the photocatalytic efficiency of TiO_2.[59,70]

In the SCS process, N or C doping is obvious because the adopted fuels usually contain these two elements and the combustion temperature is very high, which facilitates the doping of the aforementioned elements into the lattice of crystals. For example, Xiao et al.[71] prepared carbon-doped TiO_2 nanocrystals using ethylene glycol ($C_2H_6O_2$) and citric acid ($C_6H_8O_7$) as fuels. The results showed that the band gap energies (E_g) of the C-doped TiO_2 samples are about 2.90 eV, which should be attributed to two factors: (1) Ti–O–C structure in C-doped titania can be responsible for the visible-light photocatalytic activity;[72] (2) the presence of Ti^{3+} species produced in the process of carbon doping of TiO_2 leads to the formation of oxygen vacancy state between the valence band (VB) and the conduction band (CB) in the TiO_2 band structure.[73] Several groups[73,74] proved that the combustion synthesis of TiO_2 narrowed its band gap as compared to that of the commercial TiO_2, which can be attributed to the N or N,C-co-doping. Mani et al.[75] verified that among glycine, hexamine, and triethyl amine the former was the most effective fuel for improving absorbance of the co-doped TiO_2 in the visible light range.

Sivaranjani and Gopinath[76] explained the doping process with urea as a fuel. During the combustion process, urea decomposes to generate *in situ* NH_3, which acts as a nitrogen source and assures a reduction atmosphere. Embryonic titanium-oxo nanoclusters (Ti_xO_y, x/y > 1) grow in ammonia atmosphere to bigger clusters/particles with many defects. As a highly electron donating compound, ammonia easily interacts with the defect-rich clusters, which results in the incorporation of N element into TiO_2 lattice to produce $TiO_{2-x}N_x$ materials. According to the above mentioned study,[76] the urea-assisted doping procedure does not retain any organic impurities in the resulting $TiO_{2-x}N_x$ due to the complete conversion of urea to ammonia and CO_2. Moreover, the resulting materials are mesoporous structures with a high surface area (234 m^2/g). The same concept has been also adopted for making $ZnO_{1-x}N_x$.[77–79]

In addition to the possibility of selecting different fuels, another effective way for controlled doping is the usage of properly selected precursors. For example, Chen et al.[80] introduced a novel approach to the synthesis of N- and F-co-doped mesoporous TiO_2 photocatalysts using TiF_4 as a precursor, which is the source of Ti and F, and urea as a fuel and the source of N dopant.

Doping can also lead to the discovery of new energy materials. For instance, using glycine and zirconium nitrate ($Zr(NO_3)_4$•$5H_2O$), Polisetti et al.[81] synthesized C-doped tetragonal ZrO_2, which was found to be photocatalytically active with a band gap of nearly 3.5 eV. This result may provide some suggestions for the development of more effective photocatalysts by proper selection of dopants and doping conditions.

3.2.2 Formation of surface oxygen vacancies

In order to engineer efficient photocatalysts, the creation of suitable surface defects is an effective route. For instance, it was reported that the oxygen vacancies can act as electron capture centres, and hence improve the separation efficiency of charge carriers.[82-87] Oxygen vacancies can also cause the presence of a vacancy-induced band of electronic states just below the conduction band, thus narrowing the band gap of a photocatalyst.[85] In the SCS process, there is a balance between oxygen in the surrounding atmosphere and that in the crystal lattice. If the oxygen pressure in atmosphere is low enough, oxygen from the lattice would be liberated, leaving vacancies at the original lattice sites.[88,89]

A successful creation of surface oxygen vacancies is also dependent on the fuels used. If the combustion reaction releases oxygen, it is hard to acquire oxygen vacancies. Recently, our group[89] fabricated $BiOBr/Bi_{24}O_{31}Br_{10}$ nanocomposites with surface oxygen vacancies using 2-bromoethylamine hydrobromide ($C_2H_6BrN{\cdot}HBr$) as a fuel. The proposed reaction leading to the formation of BiOBr can be presented as follows:

$$Bi(NO_3)_3 \cdot 5H_2O + C_2H_6BrN \cdot HBr + 0.5CO(NH_2)_2 + 0.25O_2 \rightarrow BiOBr + 2.5CO_2 + HBr + 2.5N_2 + 4H_2O \quad (4)$$

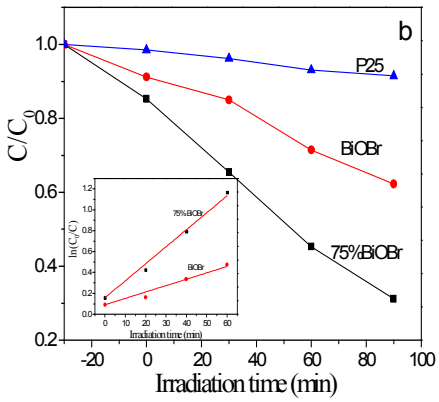

Fig. 5. Illustration of adsorption models of a) MO and b) RhB on the BiOBr surface. Reproduced with permission from ref 89 Copyright © 2013, Royal Society of Chemistry.

The ample amount of the created surface oxygen vacancies contribute to the extraordinary adsorption properties of the resulting composite, which is reflected by high adsorption capacities of both cationic dye, rhodamine B (RhB), and anionic dye, methylene orange (MO). The adsorption mechanism is shown in Fig. 5.

The influence of the fuel type and the external atmosphere on the amount of oxygen vacancies has been also verified in the case of $Bi_2Zr_2O_7$ and WO_3.[46,90] It was shown that more oxygen vacancies can lead to a narrower band gap of a given photocatalyst and higher photocatalytic activity based on the dual functions of oxygen vacancies resulting in absorbing more light and capturing photogenerated electrons.[90]

For TiO_2, the existence of oxygen vacancies is also recognized as the generation of Ti^{3+}, which can extend the photoresponse of TiO_2 from the UV to the visible light region.[91] Zuo et al.[92] demonstrated that only flammable/combustible imidazoles can generate reducing gases to convert Ti^{4+} into Ti^{3+}. Meanwhile, they found that some anions, such as Cl^-, can prohibit the formation of Ti^{3+}.

A brief survey of literature indicates that the creation of surface oxygen defects via the SCS process is an effective way of tuning the properties of catalysts, and may attract more and more attention in near future.

3.3 Doping with foreign ions

As indicated above the SCS process can sometimes result in the doping of non-metal elements such as N or/and C. To further adjust the optical structures and improve the performance of semiconductors, various metal ions can be doped into photocatalysts. Ni et al.[93] reported that the metal ion-doped TiO_2 nanoparticles *via* SCS by employing a mixture of ethanol and ethylene glycol as solvents, tetra-n-butyl titanate [$Ti(OC_4H_9)_4$] as the source of titanium in the presence of small amounts of metal ions such as Cu^{2+}, Mn^{2+}, Ce^{3+} and Sn^{4+}. The UV-vis DRS show that the absorption edges of all doped-TiO_2 samples are red shifted toward visible light region with longer wavelength as compared to those of undoped-TiO_2. They also found that the introduction of a small amount of Sn into TiO_2 increased the amount of oxygen vacancies and/or defects in the TiO_2 crystal, while in the case of doping with other metal ions an opposite effect was observed.

In Ramaswamy's work,[94] a homogeneous solid solution of $Mn_x[Ce_{0.85}Ti_{0.15}]_{1-x}O_{2-\delta}$ (x=0-0.2) was reported, which is thermally stable up to a temperature of 1050 °C; while the samples of similar composition prepared by co-precipitation or wet-impregnation methods suffer sintering at this temperature and show structural inhomogeneity. Co-doping of TiO_2 with other cerium and vanadium ions resulted in $Ti_{0.9}Ce_{0.05}V_{0.05}O$ with oxygen vacancies, as reported by Huang et al.[95]

To obtain macroporous materials, Song and coworkers[96] developed a novel electrospinning technique followed by a self-sustaining combustion procedure. The precursor of $Ce_{0.5}Zr_{0.5}O_2$ consisted of interconnected nanofibers as shown in Fig. 6a. Each nanofiber is mesoporous and the inter-connections of nanofibers form macropores. After being heated at 300 °C for 1 h, the macroporous structure is preserved, while the fiber diameters decrease obviously (Fig. 6b) owing to the decomposition of the organic matter and the formation of a solid solution of $Ce_{0.5}Zr_{0.5}O_2$.

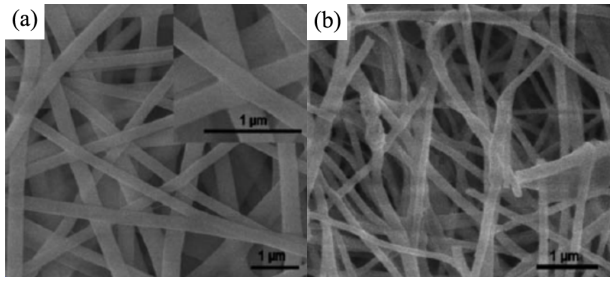

Fig. 6. (a) SEM image of the precursor of composite nanofibers of $Ce_{0.5}Zr_{0.5}O_2$ (inset: SEM image at higher magnification). (b) SEM image of $Ce_{0.5}Zr_{0.5}O_2$ nanofibers after 300 °C treatment. Reproduced with permission from ref 96 Copyright © 2011, Royal Society of Chemistry.

In many cases, doping can change the morphology of

materials. Ekambaram et al.[97] prepared co-doped ZnO and found that the un-doped ZnO particles are connected to each other in the form of a large network structure with irregular pore sizes and shapes. However, a flake-type structure was obtained for cobalt-doped ZnO. The formation of pores is due to the liberation of a large amount of gaseous products during the combustion process. Ahmad et al.[98] investigated the surface morphology of pristine ZnO and Al-doped ZnO (AZO) nanopowders. The un-doped ZnO nanoparticles were spherical and bigger, while those of AZO were smaller and ellipsoidal.

In recent decades, metal/non-metal co-doped photocatalysts have been extensively studied to improve their photocatalytic activity under visible-light irradiation.[59] Gopinath et al.[78,79] reported $(Zn_{1-z}Ga_z)(O_{1-x}N_x)$ and $(Zn_{1-z}In_z)(O_{1-x}N_x)$ solid solutions formed during SCS via Ga/In and N co-doping of ZnO with metal nitrates as the source of metal ions and urea as a fuel and the source of nitrogen. The resulting band gaps decreased to 2.5 and 2.3 eV for $(Zn_{1-z}Ga_z)(O_{1-x}N_x)$ and $(Zn_{1-z}In_z)(O_{1-x}N_x)$, respectively, because the N2p states of nitride are above O2p VB. Chen et al.[99] reported a mesoporous N, W co-doped TiO_2 photocatalyst by utilizing urea and sodium tungstate. The co-doping significantly narrowed its band gap to ca. 2.7 eV that is responsible for high visible light absorption. Furthermore, N, Cu co-doped ZnO, and N, B co-doped TiO_2 were also successfully synthesized.[100,101]

4. Synthesis of ternary and quaternary metal oxide nanomaterials

4.1 Perovskite type oxides (ABO_3)

Perovskite-type oxides (ABO_3) have attracted much attention due to their extensive applications in catalysis, photovoltaic cells, solid oxide fuel cells as energy materials and in ferroelectric random access memory, magnetic data storage, and electromechanical transducers, etc.[102] Traditional synthesis of these nanomaterials often result in undesired composition. Also, crystallization requires temperatures above 800 °C due to the difficult solid reaction between oxides. In 1993, Manoharan and Patil[103] reported the combustion synthesis of $LnCrO_3$ (Ln=La, Pr, Nd, Sm, Dy, Gd and Y) and $LaMO_3$ (M=Mn, Co, and Ni) using metal nitrates-tetraformal trisazine (TFTA) mixtures. TFTA was prepared by reacting formaldehyde and hydrazine hydrate at 0 °C under constant stirring. These oxides are of sub-micrometer size with specific surface area ranging from 3 to 20 m^2/g. This work initiated the usage of SCS for the synthesis of complex compounds.

Yttrium orthoferrite ($YFeO_3$) is a promising material for visible light photocatalytic applications due to its band gap of 2.2–2.6 eV.[104] Wu et al.[105] reported its preparation using glycine as a fuel. Chen et al.[106] obtained $YFeO_3$ and $Y_3Fe_5O_{12}$ by controlling thermal transformation with different Y/Fe initial ratios. Especially, it should be mentioned that $YFeO_3$ appears in two common phases, hexagonal and orthorhombic. Yu et al.[107] reported that the phase structure of $YFeO_3$ can be selectively controlled to be hexagonal or orthorhombic by simply adjusting the ratio of glycine to nitrate (G/N). According to their experiments, when the G/N is 0.85, $YFeO_3$ exists as an amorphous phase. As the ratio increases to 1.0 and 1.3, the phase structure is hexagonal; with the ratio of 1.5 or 1.7, the obtained $YFeO_3$ exhibits high temperature phase, orthorhombic, with a low surface area of 6-4 m^2/g. Meanwhile, the increase of glycine amount resulted in the enlargement of the particles.

Recently, $LaFeO_3$ has attracted much interest due to its high efficiency in solid oxide fuel cells and photocatalysis.[108,109] Parida[110] and Gallego[111] groups reported a sol-gel combustion synthesis of this material, which required further post-treatment at high temperature for more than 2 hours. To improve the preparation efficiency, our group[112] proposed a novel solution combustion method, the so-called self-combustion of ionic liquids. We found that some ammonium salts can coordinate with metal nitrates to form ionic liquids (ILs); meanwhile, these salts can also act as fuels in the combustion process. The ILs are mixed homogeneously at the molecular level, which is essential for the formation of nanopowders. Moreover, unlike traditional SCS, no additional water is needed to form the precursor solutions, avoiding destabilization of the system in the process of heating caused by continuous evaporation of water. In our work, ILs were prepared from $Fe(NO_3)_3{\cdot}9H_2O$, $La(NO_3)_3{\cdot}6H_2O$, and trimethylamine hydrochloride ($(C_2H_5)_3N{\cdot}HCl$). The last reagent acts as not only the source of cation in IL, but also a fuel. The resulting $LaFeO_3$ materials exhibited porous structures with quite high surface areas between 37 and 84 m^2/g. For the purpose of comparison, the surface areas of the $LaFeO_3$ samples prepared using glycine varied from 6.5 to 28 m^2/g; the highest surface area was achieved at the glycine-to-nitrate ratio of 2.[113] Wei et al.[114] also reported the synthesis of $LaFeO_3$ and $LaFe_{0.5}Mn_{0.5-x}O_3$ by stearic acid solution combustion method; the latter possessed the surface area of 38 m^2/g.

Other perovskite-type oxides, including $SrTiO_3$,[115] $BiFeO_3$,[116] $LaNiO_3$,[117] doped $BiFeO_3$,[118] and layered perovskite-type $La_4Ni_3O_{10}$[119] and γ(L)-Bi_2MoO_6[120] have been also successfully prepared via SCS, showing the suitability of SCS for the preparation of ABO_3 type compounds.

4.2 Spinel type oxide (AB_2O_4)

Spinel-type oxides (AB_2O_4) are more complex than ABO_3 and their synthesis requires higher temperatures. As a pioneer in SCS, Patil's group[8] reported the preparation of alumina-based materials, including spinel-type $MgA1_2O_4$, $CaAl_2O_4$, YAl_2O_4, and ZrO_2/AlO_2, Al_2O_3, $LaAlO_3$, and ruby powder (Cr^{3+}/Al_2O_3) by combustion of the corresponding metal nitrate-urea mixtures. The synthesis of $MgA1_2O_4$ revealed that $Mg(NO_3)_2{\cdot}6H_2O$ and $Al(NO_3)_3{\cdot}9H_2O$ exhibit different behavior with respect to urea, glycine and β-alanine.[121] It was shown that urea is the most appropriate fuel for the decomposition of $Al(NO_3)_3{\cdot}9H_2O$, while β-alanine is suitable for $Mg(NO_3)_2{\cdot}6H_2O$. As a result, the use of mixed fuels (urea and β-alanine, urea and glycine) afforded the desired materials without subsequent annealing steps. On the contrary, a single fuel (urea, glycine or β-alanine) led to the formation of an amorphous powder.

$MgAl_2O_4$ has been extensively used as a catalyst support,[122–124] humidity sensor,[125] and nuclear material[126] because of its high melting point, low thermal conductivity, high mechanical strength, good chemical inertness, and excellent radiation resistance.[121] However, there was no reference reporting its application in photocatalysis before our group reported it.[44] We showed that the photocatalytically active mixed amorphous and crystalline $MgAl_2O_4$ nanopowders can be prepared via SCS using

urea and glycine as a mixed fuel. The UV-Vis diffuse reflectance spectra of various $MgAl_2O_4$ powders are shown in Fig. 7. The observed photo-absorption can be attributed to the amorphous $MgAl_2O_4$, which features shorter Al-O bond length than that in crystalline $MgAl_2O_4$.[127]

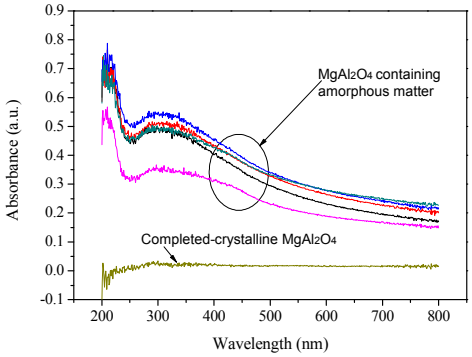

Fig. 7. UV-Vis diffuse reflectance spectra of $MgAl_2O_4$ powders. Reproduced with permission from ref 44 Copyright © 2011, Elsevier.

The Fe-based materials possess magnetic properties, which is beneficial for their recycle and reuse. Patil et al.[128] reported the synthesis of MFe_2O_4 (M=Mg, Mn, Co, Ni, Cu, Zn, Y, La, Nd, Sm, Gd, Dy, $Ni_{0.5}Zn_{0.5}$) using oxalyldihydrazide (ODH, $C_2H_6N_4O_2$) or TFTA as fuels. The combustion reaction can be controlled by adjusting heating rate and stoichiometry. A heating rate of less than 75 °C/min would not cause the occurrence of combustion and fuel-rich combustion mixtures would lead to the presence of carbon impurities. Other spinel oxides, such as doped $ZnFe_2O_4$,[129-131] $CuCr_2O_4$,[132] and $(Co,Fe)Cr_2O_4$[133] have been reported too.

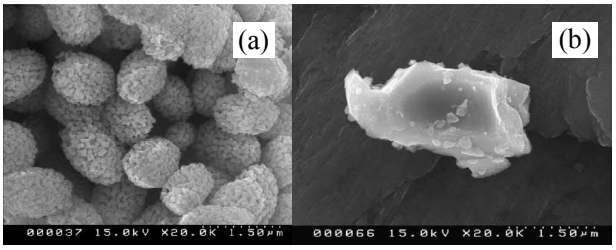

Fig. 8. FE-SEM micrographs of the $BiVO_4$ crystallites obtained via (a) SCS and (b) SSR. Reproduced with permission from ref 141 Copyright © 2008, Elsevier.

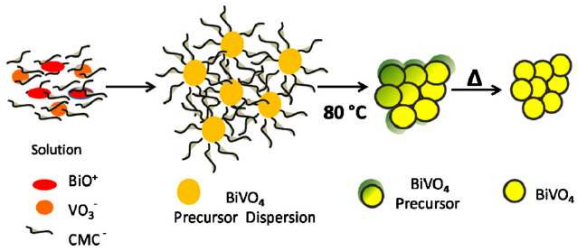

Fig. 9. Schematic illustration of the CMC-assisted formation of $BiVO_4$ nanospheres. Reproduced with permission from ref 142 Copyright © 2011, Elsevier.

To control morphology, Bao et al.[134] proposed a post-synthesis treatment method. Firstly, $CaIn_2O_4$ particles were obtained by SCS using calcium nitrate and indium nitrate as oxidizers and glycine as a fuel. Afterwards, $CaIn_2O_4$ was annealed under high temperature. During the calcination process, the nanosized grains of the as-combusted $CaIn_2O_4$ self-assembled into nanocapsules, which were further agglomerated into regular $CaIn_2O_4$ rods having the diameter of ~300 nm and the length of about 2 μm.

In conventional synthesis of ABO_3 or AB_2O_4 type compounds, intermediate products such as various oxides are always generated. SCS does not have this drawback because of homogeneous solution of the precursors used and high reaction temperature.

4.3 Scheelite type oxides (ABO_4)

Bismuth vanadate ($BiVO_4$) has attracted considerable interest because of its suitable band gap and excellent photocatalytic performance under visible-light irradiation.[135,136] There are three phases for $BiVO_4$: monoclinic scheelite, tetragonal scheelite and tetragonal zircon.[137] Among these, monoclinic scheelite-structured $BiVO_4$ with a band gap of 2.4 eV exhibits the highest photocatalytic activity under visible-light irradiation over the other forms. Urea[138] and citric acid[139,140] have been used as fuels to synthesize monoclinic $BiVO_4$ with the specific surface area around 3.0 m^2/g. Using DL-malic acid, Chandrappa et al.[137] obtained $BiVO_4$ powders possessing a large surface area of ca. 13 m^2/g.

Jiang et al.[141] prepared the spherical-shaped $BiVO_4$ photocatalysts via SCS using citric acid and urea as co-fuels followed by annealing at around 500 °C for different times. The morphologies of the resulting samples obtained via SCS and solid-state reaction (SSR) are shown in Fig. 8. As can be seen, the product obtained SCS shows uniform spherical morphology, which is not the case for the material prepared by SSR. Martinez-de la Cruz et al.[142] obtained $BiVO_4$ nanospheres in the presence of sodium carboxymethylcellulose (CMC). The spherical morphology induced by the presence of CMC is very different from that obtained by co-precipitation and solid-state reaction methods. The specific surface areas of various samples are as follows: $BiVO_4$-solid state reaction, 0.3 m^2/g; $BiVO_4$-co-precipitation, 1.5 m^2/g; $BiVO_4$-CMC200, 4.0 m^2/g, and $BiVO_4$-CMC300, 3.0 m^2/g. The proposed formation route of $BiVO_4$ nanospheres via CMC-assisted SCS method is shown in Fig. 9.

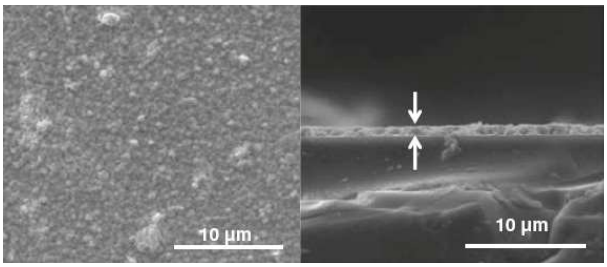

Fig. 10. SEM images of the surface and cross-section of a $BiVO_4$ film deposited on soda-lime glass substrate, with ten layers and thermally annealed at 500 °C for 1 h. Reproduced with permission from ref 144 Copyright © 2014, Elsevier.

Thin film structures are advantageous for many applications as compared to the powder morphology. $BiVO_4$ thin film has been also prepared through the solution combustion synthesis coupled with dip-coating process.[143,144] Fig. 10 shows the SEM images of $BiVO_4$ thin films. He et al.[145] immobilized $BiVO_4$ onto bentonite to obtain the $BiVO_4$/bentonite composite by SCS, which featured

larger surface area and better performance than initial $BiVO_4$, and could be easily recovered. Also, a series of other scheelite type oxides with ABO_4 structure, $FePO_4$,[146] $ZnWO_4$,[147] and $CeVO_4$[148] have been also obtained via SCS using glycine or oxalyldihidrazide as fuels.

4.4 Other complex oxides

The preparation of more complex ternary or quaternary oxides, such as Bi_2WO_6,[149] $Bi_2Ce_2O_7$,[150] $Bi_4Ti_3O_{12}$,[151] $K_{0.80}Ti_{1.733}Li_{0.267}O_4$,[152] Li_4SiO_4,[153] and Bi_4TaO_8Cl,[154] have been reported, which possess small particle sizes, relatively large specific surface areas, good crystallinity and often superior performance. Generally, the higher formation temperature and longer reaction time are required to prepare oxides with more complex structure; thus, the advantages of SCS are more obvious in the synthesis of these compounds.

Besides common fuels, some rare fuels, such as acenaphthene[155] and diformyl hydrazine[156] were also used to prepare the Li-containing compounds. Ananth et al.[155] mentioned that acenaphthene fuel was better than sucrose in reducing the particle size of $LiNi_{0.5}Mn_{0.5}O_2$ to smaller value than that of the compound prepared by simple solid state methods.

Akiyama et al.[157] reported the influence of the fuel ratio on the surface area and morphology of $Ce_{0.6}Mn_{0.3}Fe_{0.1}O_2$ (CMF) as an anode material for solid oxide fuel cells (SOFC). The samples were designated as CMF1, CMF2, and CMF3 at φ=0.5, φ=1, and φ=1.8, respectively. The BET surface areas of CMF1, CMF2, and CMF3 were estimated to be 56, 16 and 37 m^2/g, respectively, which are about 3-10 times larger than that of the SSR CMF sample, 6 m^2/g. The CMF1 sample was obtained in the form of porous particles (with pores below 50 nm), while CMF2 and CMF3 were shown to have much larger pores.

Furthermore, Huang group[158] prepared In_2TiO_5 containing octahedra [InO_6] and [TiO_6] with a band gap of 3.02 eV. The band calculations show that the open coordination environment of Ti, large dispersion of In 5s states, and the optical indirect transition are in favor of photon energy storage and electron-hole separation to benefit the photocatalytic activity of In_2TiO_5.

5. Fabrication of nanocomposites

In the case of single semiconductors there is a contradictory situation for utilizing the visible light: semiconductors with wide band gaps are not responsive to visible light, but semiconductors with narrow band gap including the modified oxides feature low charge separation efficiency, which make them ineffective photocatalysts. Combining two semiconductors with well-matched energetic levels of the valence band (VB) and conduction band (CB), where one of them can harvest visible light, to form heterojunction has been proven to be an effective method for promoting charge separation and consequently enhancing the photocatalytic efficiency.[159,160] At present, many methods have been developed to prepare hybrid photocatalysts, such as solvothermal, chemical etching, co-precipitation or precipitation–deposition, and microwave-assisted methods. Usually, one component of the composite is firstly synthesized and then was coupled with the other. As a result, the contact interface of the various compounds is limited, which is a very important factor influencing the charge carrier transfer efficiency. However, one-pot preparation of heterostructured products from distinct starting materials is difficult because of their different growth mechanisms and reaction rates. Hence, combining different components to engineer complex hybrid photocatalysts with proper interface remains as a challenging but exciting topic.[161]

Again, SCS has unique advantages for fabrication of hybrid photocatalysts. It can assure high homogeneity of mixed precursors and narrow size distribution, which benefit the preparation of chemically homogenous, uniform and well-dispersed heterojunctions with more active contact sites, thus improving the charge transfer efficiency.[162]

5.1 Heterostructured metal oxides

5.1.1 Support immersion synthesis

Support-assisted immersion synthesis involves infiltrating the pre-prepared component with the precursor solution prepared for combustion. At high temperature generated by the exothermic reaction or calcination, two or more components are combined firmly to form heterojunctions. For example, as mentioned in section 4.3, $BiVO_4$ is a potential photocatalyst in energy-related applications. However, its low quantum efficiency restricts further applications of this material. Jiang et al.[163] obtained $CuO/BiVO_4$ composite photocatalysts by incipient wetness impregnation technique. Firstly, $BiVO_4$ was prepared by a combustion method using citric acid and urea as co-fuels. Then, $BiVO_4$ was mixed with water and $Cu(NO_3)_2{\cdot}3H_2O$ to obtain a paste. Finally, the paste was dried and annealed to form $CuO/BiVO_4$ composite. As for TiO_2, various semiconductors with narrower band gap have been combined with TiO_2 to improve its quantum efficiency and the visible-light absorption ability. For instance, an infrared-to-ultraviolet upconversion agent Y_2O_3:Yb^{3+}, Tm^{3+} and a novel composite photocatalyst TiO_2/Y_2O_3:Yb^{3+},Tm^{3+} have been synthesized by combustion and precipitation methods.[164]

Recently, graphene oxide (GO) has attracted a lot of attention as a good candidate for supporting nanoparticles in liquid phase, which can facilitate the transfer of photo-generated electrons from photocatalysts to GO due to its excellent electronic conductivity, and thus reduce the recombination of charge carriers.[165] Moreover, the high surface area of GO is beneficial for adsorption of reactants and their diffusion to the photocatalyst. Naturally, GO was selected to combine with TiO_2,[165,166] $CoFe_2O_4$[167] and $NiFe_2O_4$.[168]

Generally, the specific surface area of the composites after combustion should be lower than that of the components before combustion. For instance, when α-Al_2O_3, γ-Al_2O_3, and ZrO_2 were used as porous supports, the specific surface areas of the supported catalysts were about or below the surface areas of the supports. However, Mukasyan et al.[169] observed that the surface area of combusted Fe_2O_3/activated Al_2O_3 increases as compared to that of the support. They thought that the decrease of reaction temperature caused by the water evaporation from activated Al_2O_3 and intensification of gas-phase evolution in the combustion wave led to an increase in the surface area of the composite products. The former restricts kinetics of the growth of nuclei and the latter hinders the collision between formed solid nuclei. In the case of α-Al_2O_3, γ-Al_2O_3, and ZrO_2, the decrease in

the surface area of the loaded catalysts may be due to the "epitaxial" coverage of the support surface and the sintering at high combustion temperature.

Inspired by above result and previous research that amorphous $MgAl_2O_4$ has shorter Al-O bond length and narrower band gap,[44] our group[43] developed TiO_2/amorphous Al_2O_3 composite containing amorphous Al_2O_3 ingredient, which shows ultraviolet light response ability. To obtain TiO_2/Al_2O_3, commercial P25 TiO_2 was immersed in the solutions of $Al(NO_3)_3{\cdot}9H_2O$, urea, and water; then the suspension was heated to carry out the combustion. The resulting hybrids exhibited interesting properties: firstly, N element contained in urea was introduced (doped) into the lattice of TiO_2, which resulted in the shift of light absorbance of TiO_2 from red to visible region; secondly, the composite exhibited much higher surface area (the highest was 161 m^2/g) than that of P25 (46 m^2/g); thirdly, the photocatalytic activity of the hetero-junction was greatly enhanced due to the larger amount of defect sites on amorphous Al_2O_3 that can transfer electrons from TiO_2. In this combustion process, TiO_2 was used as support; while from the photocatalysis viewpoint, Al_2O_3 acts as an active support. Hence, this combustion method can be called "reverse support combustion".

However, the support-assisted immersion synthesis is not an in situ process and the contact area of the components is also limited. Therefore, it is highly desirable to develop more effective methods for enhancing transfer efficiency of charge carriers.

5.1.2 One-step preparation from homogeneous solution

In SCS, hybrids can be obtained by using a homogeneous solution of precursors. The high temperature of combustion can cause a simultaneous formation of various metal oxides. In order to obtain TiO_2-based heterostructures, Reddy et al.[170] employed titanyl nitrate ($TiO(NO_3)_2$) formed by the reaction of titanium iso-propoxide with nitric acid, zirconyl nitrate ($ZrO(NO_3)_2$), siliconyl nitrate obtained by reacting tetraethyl orthosilicate (TEOS) with nitric acid, aluminum nitrate nona-hydrate ($Al(NO_3)_3{\cdot}9H_2O$) as precursors and urea as a fuel to prepare TiO_2–SiO_2, TiO_2–Al_2O_3, and TiO_2–ZrO_2 mixed oxides, which were found to be quite thermally stable (i.e., no phase transformation from anatase to rutile) and showed high surface area ranging from 89 to 115 m^2/g. By varying the amount and type of metal nitrates, α-Bi_2O_3/Bi_2WO_6,[171] $Sm_2Ti_2O_7/SmCrO_3$,[172] $Gd_2Ti_2O_7/GdCrO_3$,[173] ZnO/Fe_2O_3,[174] and $V_2O_5/BiVO_4$[175] have been also developed.

In the combustion process, when the amount of oxygen is insufficient or the fuel is in excess, the combustion reaction would be incomplete, which can result in the presence of carbonaceous impurities in the resulting materials. For example, Falaras et al.[176] modified TiO_2 by controlling the urea content and calcination temperature, thus reaching an absorption threshold of 2.19 eV. The visible light absorption of TiO_2 was ascribed to the existence of monolayer of carbonaceous species, which covered the surface of TiO_2 anatase nanoparticles.

On the other hand, it should be stated that there is also disadvantage of one-step *in situ* preparation of hybrid photocatalysts. Because of homogeneous composition, very high reaction temperature, unexpected intermediate products, additional phases, such as $CeAlO_3$ in CeO_2/Al_2O_3 system and Al_2O_3 in $CeO_2/CeAlO_3$ composites are often formed.[177,178] In some cases, it is difficult to adjust the reaction conditions to avoid the formation of by-products.

The aforementioned hybrids are composed of two kinds of oxides. It is known that some metal oxides own many phases (polymorphism) or compositions. For example, iron oxides can exist as Fe_3O_4 or four different Fe_2O_3 phases:[179] α-, β-, ε-, and γ-Fe_2O_3. Iron oxides with different phases possess various band gap energies. Sometimes it is desirable to prepare composites with mixed-phase or composition derived from the same oxide family. However, some phases are metastable and it is hard to obtain such hybrids using traditional synthesis methods because their long reaction time will affect the stability of the metastable phases; in this case SCS is the method of choice for the synthesis of mixed-phase oxides. Our group[20] reported mixed-phase Fe_2O_3 with α and β structures via self-combustion of ILs using $(C_2H_5)_3N{\cdot}HCl$ as a fuel. The β/α-Fe_2O_3 ratio was controlled by adjusting the fuel amount; this ratio decreased with increasing the amount of fuel. This method afforded the metastable β-Fe_2O_3. Other analogous composites, such as (α+γ)-Fe_2O_3,[28] Fe_2O_3/Fe_3O_4,[27,39] and CoO/Co_3O_4,[22] were also synthesized by varying the fuel amount or calcination atmosphere.

In recent years, BiOCl has attracted much attention due to its good photocatalytic activity under UV irradiation since Zhang et al. reported its high efficiency in photodegradation of methyl orange.[180] However, the band gap of BiOCl is in the range of 3.19–3.60 eV, which is too large for efficient utilization of solar energy. $Bi_{24}O_{31}Cl_{10}$ with the band gap of ca. 2.90 eV is a product of the thermal decomposition of BiOCl.[181] Our group[21] fabricated $Bi_{24}O_{31}Cl_{10}$/BiOCl heterojunctions via the self-combustion of ILs, which were prepared from $Bi(NO_3)_3$ and diethylamine hydrochloride ($(C_2H_5)_2NH{\cdot}HCl$). The latter is not only the cation in IL, but also the main fuel in the combustion process. The ratio of $Bi_{24}O_{31}Cl_{10}$ to BiOCl can be controlled by adjusting the ratio of $(C_2H_5)_2NH{\cdot}HCl$ to urea, which acts as an additional fuel.

5.2 Metal supported inorganic oxides

Transition metals have been widely used as co-catalysts for enhancing the electron transfer efficiency of photocatalysts. Especially the surface plasmon resonance (SPR) properties of noble metals make them responsive to visible light. Therefore, deposition of noble metals on the surface of photocatalysts can be used to make them responsive to visible light. In SCS, metal nanoparticles can be *in situ* generated by reducing metal oxides in a reductive atmosphere that can be created by the excess of fuels,[30] for instance by ammonia formed due to the decomposition of urea as shown by the following equations:[182,183]

$$CO(NH_2)_2 \rightarrow NH_3 + HCNO \quad (5)$$

$$NiO + NH_3 \rightarrow Ni + H_2O + N_2 \quad (T > 450\ ^oC) \quad (6)$$

By selecting an appropriate fuel and controlling atmosphere, inorganic oxides loaded with metal nanoparticles, such as Pd, Pt, Ag, Cu, and Ni on TiO_2, ZnO, CeO_2, Al_2O_3, NiO, can be prepared by using SCS.[33,183–195] The formed heterojunctions exhibit much better performance than those present in the traditionally prepared composites due to a very good dispersion of metal particles in porous oxides.

On the other hand, it is well known that the size and amount of the loaded metal particles are important factors that influence the performance of the composite photocatalysts. However, it is

difficult to precisely estimate the size and amount of the deposited metal particles, which is a drawback of SCS.

6. Energy storage and conversion

6.1 Energy storage

6.1.1 Electrode materials for lithium-ion batteries

To efficiently generate the clean and safe electric power, the development of highly efficient energy storage devices is an important task. Li-ion rechargeable battery (LIB) is a device converting chemical energy to electrical energy, which has been widely used in mobile phones, laptops, digital cameras, and medical microelectronic devices thanks to its high energy density and long cycle life.[13,196,197] An electrochemical cell is composed of two electrodes, the negative electrode (anode) and the positive electrode (cathode), separated and connected by a Li^+ conducting electrolyte. The LIB performance including the specific energy and power, cycle life, and discharge rates rely largely on the intrinsic chemistry of cathode and anode materials. When the LIB is working, chemical potential is converted into electrical energy via Faradaic reactions, which is affected by the composition, crystal structure, and morphology of the electrodes.[198] Hence, great efforts have been recently undertaken to improve the electrode materials, especially cathode materials, because cathodes affect the cell voltage, charge transfer kinetics, safety, and cost.[199]

Lithium cobalt oxide ($LiCoO_2$) is a common commercial cathode material assuring high voltage, good reversibility, and high theoretical specific capacity of Li-ion batteries. $LiCoO_2$ has a layered rhombohedral structure with lithium atoms in the 3a, cobalt atoms in 3b, and oxygen atoms in 6c positions (with respect to hexagonal axes).[200] Both Rodrigues[156] and Kalyani[201] groups verified that $LiCoO_2$ obtained by SCS features the first discharge capacity of over 120 mAh g^{-1} and a less than 10% capacity fade after 30 cycles. However, high cost, and toxicity of cobalt, limited rate capability and safety concerns of $LiCoO_2$ restrict its further applications. To tackle these problems, the ion-doped $LiCoO_2$ materials have been proposed; for example, $LiCo_{1-x}Ni_xO_2$,[202,203] $LiCo_{0.6}Ni_{0.2}Mn_{0.2}O_2$,[204] show higher specific discharge capacity and good cycle-life performance.

As alternative cathode materials with smaller toxicity, the olivine-type and layered manganese-based materials have attracted much attention. Hong et al.[205] reported that a multi-metal oxide $Li[Mn_{0.547}Ni_{0.16}Co_{0.10}Li_{0.193}]O_2$ solid solution delivered the first discharge capacity of 265 mAh g^{-1} between 4.8 to 2.0 V at the specific current of 100mA g^{-1}. Ananth's group[154] prepared $LiMn_{0.5}Ni_{0.5}O_2$ via SCS, which exhibited an initial discharge capacity of 161 mAh g^{-1} in a voltage range of 4.6–2.5 V at 0.1 C (1 C is defined as one lithium per formula in one hour) rate and can be subjected to more than 50 cycles. This desirable electrochemical property can be attributed to the pure phase of $LiNi_{0.5}Mn_{0.5}O_2$, which is difficult to prepare especially by the conventional solid state fusion method.[206,207] However, Park et al.[208] explored a simple combustion method for the synthesis of $Li[Mn_{(2/3-x/3)}Ni_xLi_{(1/3-2x/3)}]O_2$ compounds with low Ni content. Based on the XRD and electrochemical data they concluded that $LiMn_{0.5}Ni_{0.5}O_2$ exhibited a relatively low initial discharge capacity of 200 mAh g^{-1} and a large loss in the capacity during cycling; while $Li[Mn_{0.61}Ni_{0.17}Li_{0.22}]O_2$ and $Li[Mn_{0.58}Ni_{0.25}Li_{0.17}]O_2$ solid solutions featured high initial discharge capacities of over 245 mAh g^{-1} and a stable cycle performance between 4.8–2.0 V. Aurbach's group[209] obtained $LiNi_{0.5}Mn_{0.5}O_2$, $LiNi_{0.33}Mn_{0.33}Co_{0.33}O_2$ and $LiNi_{0.4}Mn_{0.4}Co_{0.2}O_2$ cathode materials with the capacity of 190, 180 and 170mAhg^{-1}, respectively, via self-combustion reaction following by calcination; while their rate capability (discharge capacity *vs.* cycle number at different C rates) follows the order as below: $LiNi_{0.33}Mn_{0.33}Co_{0.33}O_2$< $LiNi_{0.4}Mn_{0.4}Co_{0.2}O_2$<< $LiNi_{0.5}Mn_{0.5}O_2$. The spinel-type lithium manganate ($LiMn_2O_4$) also serves as high-capacity intercalation cathode for rechargeable lithium-ion batteries due to its economic and environmental advantages.[210-212] $LiMn_2O_4$ can be synthesized via SCS and its electrochemical behavior is reported elsewhere.[210,213] To reduce the capacity fading at elevated temperatures and during overcharge of $LiMn_2O_4$ powder-based electrodes, Novak et al.[214] developed nanostructured $LiMn_2O_4$ thin films by flame spray deposition and *in situ* annealing via igniting and depositing precursor solution. The obtained $LiMn_2O_4$ film exhibited good cyclability.

Besides the aforementioned cathode materials, Goodenough et al.[215] explored lithium iron phosphate ($LiFePO_4$) as a cathode. Shao et al.[216] reported the preparation of $LiFePO_4$ at an optimal glycine/$LiFePO_4$ ratio of 4:1 using inexpensive iron (III) as a precursor. The obtained material exhibited the discharge capacity of 100 mA h g^{-1} at a 0.1 C rate. Govindaraj et al.[217] reported also another phosphate, $LiNiPO_4$ doped with Cu^{2+} and Mg^{2+} ions via SCS. They found that the ionic conductivity increased at lower concentrations of dopants due to the increased channel size for Li^+ diffusion; however, the ionic conductivity decreased with increasing dopant concentration due to inherent anti-site defects.

Carbon materials are frequently applied to improve the electrochemical performance of electrode materials in lithium-ion batteries.[218–223] In the case of the solution combustion synthesis, solid carbon can be in situ generated as a primary product from fuel under fuel-rich conditions or in reductive atmosphere; hence, the electrical conductivity of the electrodes can be enhanced. For example, Shao et al.[216] further treated $LiFePO_4$ with sucrose as carbon source after auto-combustion. They greatly increased the discharge capacity of the $LiFePO_4$/C sample containing about 2.86 wt.% carbon to 160 mA h g^{-1} at a 0.1 C rate and 110 mA h g^{-1} at a 5 C rate. In addition, the electrodes show excellent cycling performance during 90 cycles at various rates. Kalaiselvi et al.[224] employed ODH as a combustible fuel and a carbon source to prepare $Li_3M_xV_{2-x}(PO_4)_3$/C (M=Fe, Co) composite to further enhance the electronic conductivity and lithium transport kinetics based on the fact that native $Li_3V_2(PO_4)_3$ has a high theoretical capacity of 197 mA h g^{-1}. The combined effect of residual carbon from ODH and the added super P carbon (a kind of commercial carbon) led to the formation of carbon wiring. $Li_3Co_{0.10}V_{1.90}(PO_4)_3$/C showed the highest capacity (178 mAh g^{-1}) and very little fade (4%) after 50 cycles under a 10 C rate due to the synergistic effect of the present carbon and the optimum concentration of Co substituent.

As negative-electrode materials, cobalt oxides (Co_3O_4 and CoO) have also attracted great interest because of their high theoretical specific capacity (890 mAh g^{-1} for Co_3O_4 and 715 mAh g^{-1} for CoO).[225,226] However, the high cost of cobalt oxides

as compared to other transition-metal oxides diminishes their application value, which, in part, can be counterbalanced by a low cost synthesis route. Hence, Wu and co-workers[227] synthesized Co_3O_4/CoO composite by facile and inexpensive SCS and investigated its performance in LIBs. They verified that the composite obtained in the presence of NaF exhibited higher discharge capacity, higher initial Columbic efficiency, and better cycling performance than that achieved for the material without NaF.

The commercially applied graphite anode materials have a low theoretical capacity of 372 mAh g^{-1} and a poor safety caused by the low voltage plateau (about 0.1 V vs Li/Li^+).[228] Therefore, nano-structured metal oxide anodes have attracted a lot of interest because of their chemical stability and high capacity aimed at replacement of graphite anode materials.[229–232] Using SCS in the presence of NaF, Wu et al. [233] obtained NiO/Ni nanoparticles as an anode material according to the following reaction mechanism.[225]

$$NiO + 2Li \underset{charge}{\overset{discharge}{\Leftrightarrow}} Li_2O + Ni \quad (7)$$

NiO/Ni nanoparticles have a charge capacity of 743 mAh g^{-1} and the capacity at the end of 20th cycle is 702 mAh g^{-1} with a retention of 94%. Moreover, the coulomb efficiency with a high initial value of 70.8% keeps this value over 96% during cycling. As compared to the capacity of nanosheet-based NiO microspheres, which decreased sharply to 50 mA g^{-1} after 8 cycles,[234] they indicated that nanoparticles are better due to the shorter diffusion lengths for Li^+, and enhanced electric conductivity by the presence of Ni. Meanwhile, the fluffy porous structure generated by the released gases during combustion process not only buffers the volume change during cycling but also benefits the efficient entrance and permeation of the electrolyte into the electrode and diffusion of ions.

Iron oxides are also promising anode materials because of their high theoretical capacity (1007 mAh g^{-1} for Fe_2O_3, 924 mAh g^{-1} for Fe_3O_4), non-toxicity, low cost, good safety, environmental friendliness and high resistance to corrosion.[226,235,236] Liang et al.[235] constructed Fe_2O_3/C nanocomposite by simply increasing the dosage of citric acid in the precursor solution. The as-prepared Fe_2O_3/C composite exhibited high reversible capacities of 470 and 419 mAh g^{-1} at 80th and 200th cycles with a current density of 125 mAh g^{-1}, which are much higher than those of the counterparts without carbon (i.e., Fe_2O_3 nanoparticles), which can be ascribed to the in situ formed carbon, well-developed mesopores and relatively high specific surface area achieved by SCS.

Complex oxides are useful as anode materials; for instance, nanosized spinel $Li_4Ti_5O_{12}$ (LTO) prepared via combustion synthesis exhibited high electrochemical performance and fairly stable cycling performance because of the good crystallinity and high phase purity. Shukla et al.[237] compared the influence of the synthesis methods on the capacity of LTO. The recorded capacities for the combusted LTO were equal to 125, 102, 90, and 70 mA h/g at 25, 50, 80, and 100C rates, respectively; these values are higher than those measured for nanosized LTO prepared by a solid-state method (see Fig. 11). An analogous finding was also reported by Yuan et al.[238] Thus, high crystallinity and phase purity, large specific surface area, and high porosity of the electrodes (as shown in Fig. 12) facilitate the diffusion of Li species and the electrolyte percolation through porous structure, which ensures a high flux of Li ions. Li et al.[239] further modified LTO with nitrogen (N-LTO) and showed that N-LTO with 1.1 wt % of nitrogen featured higher rate capability and better reversibility as compared to pristine LTO. The superior electrochemical performance of N-LTO was ascribed to its porous structure and nitrogen modification, which facilitate the transfer of ions and electrons. Li et al.[240] also verified the effectiveness of porous anodes in rechargeable lithium-ion batteries in the case of $Li_2MTi_3O_8$ (M=Zn, Co) flakes obtained via one-step solution-combustion.

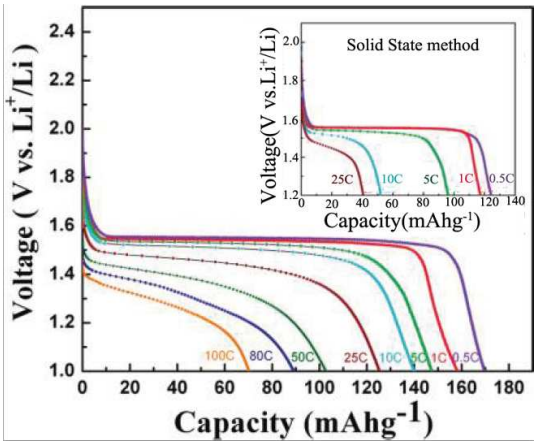

Fig. 11. Capacity-voltage profiles for nanocrystalline $Li_4Ti_5O_{12}$ synthesized by the combustion method at different rates. Inset shows the capacity voltage profile for bulk $Li_4Ti_5O_{12}$ prepared by a solid-state method. Reproduced with permission from ref 237 Copyright © 2010, American Chemical Society.

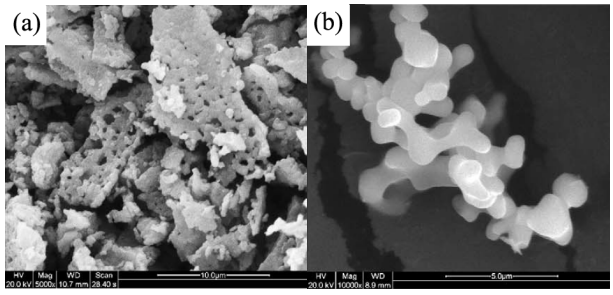

Fig. 12. SEM images of $Li_4Ti_5O_{12}$ prepared via (a) solution combustion, and (b) solid-state reaction. Reproduced with permission from ref. 238 Copyright © 2008, Elsevier.

In future, the development of electrode materials should be directed toward improvement of their structural stability and charge carrier transport by reducing the size of particles to the nanometer level.[241] Also, the design of well-developed porosity and ion doping are essential for the fabrication of highly performing electrode materials.[241,242] SCS is the well suited method for achieving electrode materials with the desired properties for Li-ion batteries.

6.1.2 Electrode materials for supercapacitors

Supercapacitors (SCs), also known as ultracapacitors, or electrochemical capacitors, have attracted a great interest due to

their high energy density, long cycle life (>100 000 cycles), simple principle, and high dynamic of charge propagation.[243,244] Generally, the electrode materials for supercapacitors can be categorized into three principal types: electrical double layer-based electrodes such as porous carbons and graphene, Faradic reaction-based electrodes such as metal oxides/hydroxides and conductive polymers.[245,246] Transition metal oxides based on Faradaic redox reactions have been widely studied due to their potentially higher capacitance as compared to porous carbon materials, mainly originating from their multiple oxidation states. However, the intrinsically low electrical conductivity and the fact that fast Faradaic reactions only occur on the surface of oxides restrict their applications.[247] Therefore, the development of nanostructured porous materials is of high priority. Based on the fact that $CuCo_2O_4$ nanostructures have been used as anode in Li-ion batteries with high Li-ion storage capacities,[248,249] Mousavi et al.[247] prepared cauliflower-like nanostructured $CuCo_2O_4$ via urea combustion method combined with a post annealing process. The resulting material possessed a high capacitance of 338 F g^{-1} at 1 A g^{-1} (8 times greater than that of $CuCo_2O_4$ microparticles) and exhibited capacitance of 88 F g^{-1} at an extremely high current density of 50 A g^{-1}, with a high power density of 22.11 kW kg^{-1}. Furthermore, 5000 continuous cycles performed at various current loads demonstrate its electrochemical suitability as a promising electrode material for high-rate SC.

Recently, metal molybdates have been used as electrode materials in Li-ion batteries[250,251] and SCs.[252–254] After combustion synthesis of $MnMoO_4$, $CoMoO_4{\cdot}xH_2O$ and $NiMoO_4$ with specific capacitance of 126, 401 and 1116 Fg^{-1} at 5 mA cm^{-2}, respectively,[255] Selvan et al.[256] prepared β-$NiMoO_4$–$CoMoO_4{\cdot}xH_2O$ nanocomposites via SCS and verified that $NiMoO_4$–$CoMoO_4{\cdot}xH_2O$ nanocomposite with Ni : Co ratio 3 : 1 exhibited a capacitance of 1472 Fg^{-1} at a current density of 5 mA cm^{-2}. They attributed this excellent electrochemical capacitance behavior to uniform small particle sizes, high specific surface area and increased electronic conductivity.

Metal oxides containing lithium have been reported as electrode materials in supercapacitors.[257,258] Among all the lithium insertion compounds, the spinel-type $LiMn_2O_4$ materials are economically feasible and environmentally friendly. To eliminate a severe reduction in the capacity during long-term cycling, Wang et al.[259] prepared Cr-substituted $LiMn_2O_4$ samples by urea-assisted combustion method and found that the partial substitution of Mn^{3+} by Cr^{3+} can increase the stability of the spinel structure and improve the cycling performance. Kim et al.[260] also reported that $Li_4Mn_5O_{12}$ obtained by combustion synthesis showed good properties because of its large specific surface area.

Similar to the utilization of carbon as additive/support in rechargeable Li-batteries, the electrode materials with carbon introduced by in situ or ex-situ processes have been also developed for SCs to enhance their electrical performance and durability. For example, ZnO/C,[261] Fe_2O_3/C, Fe_2O_3-SnO_2/C, and Fe_2O_3-ZnO/C[262] were synthesized by Jayalakshmi group via SCS.

Efficient electrode materials for supercapacitors should feature narrow particle size distribution and high specific surface area. Therefore, to develop more efficient electrodes, the pore sizes and pore distribution should be controlled, which cannot be achieved without good understanding of the solution combustion synthesis.

6.2 Energy conversion

Energy conversion refers to the transformation of energy from one form to another, for example, solar energy to chemical or electrical, electrical to chemical or mechanical energy.[13] With the ever-increasing rapid depletion of fossil fuels, energy issue became one of the most important and challenging topics in the world. Advanced energy conversion devices (including artificial photosynthesis catalysts, fuel cells, and solar cells) are expected to play an important role in utilizing the clean and safe solar energy.[263] The development of low cost, highly efficient new materials is the key for successful application of energy conversion devices. In this section, the application of nanomaterials, obtained via SCS method, for energy conversion is reviewed.

6.2.1 Artificial photosynthesis

Artificial photosynthesis mainly refers to the conversion of photon energy into chemical energy. For example, solar fuels such as hydrogen, methanol or formic acid, can be obtained by water splitting or by photocatalytic and photoelectrochemical CO_2 reduction.[264-268] As regards the CO_2 reduction, Ye group[83] reported a self-doped $SrTiO_{3-\delta}$ obtained by a carbon-free one-step combustion method and subsequent thermal treatments in Ar. They demonstrated that higher oxygen deficiency is beneficial for chemical adsorption of CO_2 on the surface and in the bulk of $SrTiO_{3-\delta}$, especially for accommodation of CO_2 in oxygen vacancies, which improves the artificial photosynthesis efficiency for methanol production.

Ye's work explains clearly that the structure of the SCS-generated material affects its performance. However, due to the complexity and diversity of morphologies and structures of the SCS-generated materials, sometimes, it is difficult to establish their influence on the catalytic activity. For example, Groven et al.[269] reported that the hydrogen generation rate over Co_3O_4 prepared via SCS in the presence of $NaBH_4$ was about twice higher than that obtained over commercial Co_3O_4, though their specific surface areas are comparable. They attributed the observed significant enhancement due to the foam-like morphology achieved via SCS method, which may facilitate the effective conversion of Co_3O_4 to the active catalyst, cobalt boride, derived via reaction between Co_3O_4 and $NaBH_4$.

Besides the structure effect, the chemical composition is also important. Gomathisankar et al.[234] prepared B-doped ZnO via SCS, the photocatalytic activity of which for H_2 evolution from aqueous Na_2S + Na_2SO_3 solution was shown to be about twice higher than that of undoped ZnO. The role of B was ascribed to the improved separation efficiency of the photoexcited electron/hole pairs and the formation of new B_2O_3. The authors also proposed an in situ formation of p-n heterojunctions. The p-type ZnS formed from photoreduced Zn^{2+} and S^{2-} was coated on the surface of n-type B/ZnO to form B/ZnO-ZnS.

6.2.2 Electrode materials in fuel cells

Solid oxide fuel cells (SOFCs) are considered as efficient energy conversion devices with the advantage of direct usage of hydrocarbon fuels. SOFCs consist of two porous electrodes, anode and cathode, separated by a dense solid oxygen ion

conducting electrolyte. On the cathode (air electrode) side, oxygen is reduced to oxygen ion, which is transported through the electrolyte to the anode.[270]

In the most frequently used SOFCs system, Y_2O_3 stabilized ZrO_2 (YSZ) is usually employed as an electrolyte, the cermet-like Ni-YSZ as anode, and electronically conducting oxides such as lanthanum manganites or $LaCoO_3$ as cathode.[271]

In the case of Ni-YSZ anode, Ni tends to sinter and agglomerate at the high SOFCs operation temperature of nearly 1000 °C, which would decrease the anode performance. Furthermore, coke deposition and sulfur poisoning reduce the anode properties in the presence of gas as an anode fuel.[157] To minimize these disadvantages, various oxides have been explored, such as fluorite, perovskite, tungsten bronze, and pyrochlore types, etc.[270,272]

As a fluorite-type compound, CeO_2 has been used as anode in SOFCs. To further improve its electrical properties and/or chemical stability against reduction under open-circuit voltage (OCV) conditions, ion doping and cermet-like materials have been used.[108,273] Zhu et al.[157] prepared via SCS method $Ce_{0.6}Mn_{0.3}Fe_{0.1}O_2$ (CMF) anode for SOFC and compared it with the conventional SSR sample. This comparison shows that the SCS product exhibited the power densities of 1.23 W cm^{-2} at 1000 °C under configuration of the cell of CMF/$La_{0.8}Sr_{0.2}Ga_{0.8}Mg_{0.15}Co_{0.05}O_3$/$Sm_{0.5}Sr_{0.5}CoO_3$ using humidified hydrogen gas as a fuel and O_2 as an oxidizing agent, which is higher than 1.09 W cm^{-2} for the SSR-derived sample under the same evaluation conditions.

In direct methanol fuel cell (DMFC), the reaction intermediate, CO, would strongly binds to the catalyst surface and occupies the active sites during the process of low temperature oxidation of the fuel. Among different approaches for solving this problem, the use of a Pt-Ru alloy was shown to be successful. To reduce the cost by replacing the use of noble metals, Mukasyan et al.[274] prepared $LaRuO_3$-Pt and $SrRuO_3$-Pt composites via SCS, which contained four times less platinum, and displayed a comparable apparent catalytic activity to that of a standard Pt-Ru alloy.

To decrease the high operation temperature, it is necessary to develop solid electrolytes having high ionic conductivity at intermediate temperatures. Doped-CeO_2 solid solutions have been widely reported as promising low temperature electrolytes.[275-277] Parkash et al.[278]reported that $Ce_{0.82}Sm_{0.16}Sr_{0.02}O_{1.90}$ prepared via SCS and post-calcination exhibited the conductivity of 2.67×10^{-2} S cm^{-1} at 600 °C. Aruna et al.[279] prepared $Ce_{0.8}Gd_{0.2}O_2$ powders using oxalyl dihydrazide as fuel with conductivity of 3×10^{-4} S cm^{-1} at 400 °C). Park et al.[280] compared the performance of Nd-doped ceria electrolytes obtained via solid state, combustion, co-precipitation and hydrothermal synthesis. The results show that $Nd_{0.2}Ce_{0.9}O_2$ and $Nd_{0.1}Ce_{0.9}O_2$ intermediate temperature-solid oxide electrolytes synthesized by combustion method and sintered at 1450 °C for 4 h featured the highest ionic conductivities in air at 600 °C and below 550 °C, respectively.

In the development of cathode materials via SCS for intermediate temperature SOFCs, Jiang et al.[281] prepared $La_{0.8}Sr_{0.2}Co_{0.8}Ni_{0.2}O_3$ (LSCN) nanopowders. Next, the chemical compatibility of LSCN, YSZ and Gd_2O_3 doped CeO_2 (GDC), and electrochemical activity of LSCN were evaluated. The results show that LSCN is compatible with YSZ at temperatures below 850 °C, and its electrode area specific resistance (ASR) is 0.30 and 0.10 Ω cm^2 at 700 and 750 °C, respectively, indicating its potential as an alternative cathode material for intermediate temperature SOFCs. Akiyama et al.[282] produced $LaMO_3$ (M: Fe, Co, Mn) perovskite type oxides and tested their electrocatalytic activities for oxygen reduction reaction (ORR) and oxygen evolution reaction (OER) using a three-electrode half-cell design and a full rechargeable Zn-air battery with a 6 M KOH electrolyte. Electrochemical characterization showed that the order of activity is as follows: $LaMnO_3$ > $LaCoO_3$ > $LaFeO_3$ > CB (carbon black). However, $LaMnO_3$-catalyzed air electrode degraded very quickly in the cycling performance measurements, whereas the $LaCoO_3$-based electrode showed the best recharge ability and stability.

Cathode or electrolyte materials in SOFCs require appropriate chemical compositions, lattice parameter (adjusted by dopant type and content), and structure (particle size, microstructure).

6.2.3 Photovoltaic solar cells

As the most important source of renewable energy, solar light can be used directly either as the heat source or converted into electrical energy by photovoltaic cells.[283] Over the past several decades, crystalline silicon and thin film solar cells, known as the first and second generation solar cells, were used. As compared to silicon cells, thin films are less costly, however, show lower efficiency.[284] To develop the third generation high-performance photovoltaic solar cells, various nanostructure-based semiconductors are needed to convert sunlight into clean electrical power.[285] The need for low-cost semiconductors open new opportunities to SCS as a facile and energy-saving method.

Among several different types of solar cells, dye sensitized solar cells (DSSC) have been considered as a highly promising device due to their simple fabrication process, low production cost and high photoelectrical conversion efficiency.[286] In DSSC, dye molecules are adsorbed on a TiO_2 thin film photoelectrode, which is attached to a piece of transparent conducting oxide (TCO) glass, and the photo-generated electrons of dyes can be injected to the CB of TiO_2 film, and then transferred to the TCO glass and external circuit. Hence, the absorbance ability of TiO_2 films is a very important factor influencing the electron transfer and photoelectrical conversion efficiency, the requirement for these films is their high porosity and nanosized structure.[287] Chung et al. synthesized TiO_2 nanopowders by SCS and fabricated photoelectrodes using them in DSSCs. Their study indicates that the aforementioned nanopowder shows similar performance as commercial P25 TiO_2 and can work well as photoelectrode in DSSCs.

Polymer solar cells (PSCs) have attracted a great attention due to their low-cost and wide applications from flexible and low-weight solar modules to photon recycling in liquid-crystal displays.[288,289] Li et al.[290] prepared a solution-processed molybdenum oxide (MoO_3) hole selective layer via SCS. The obtained MoO_3 hole selective layer exhibited high charge transportation ability similar to that of poly-(ethylenedioxythiophene):polystyrene sulfonate (PEDOT:PSS); meanwhile, it possessed better device stability. The hole-transport layers (HTLs) are of great importance for solution-processed optoelectronic devices to improve the efficiency of the charge extraction/injection and increase device stability.[291–293] Jin et al.[294]

fabricated NiO_x thin films via SCS. When these films were used as HTLs in the solution-processed optoelectronic devices such as heterojunction organic photovoltaics with a model system of poly[2,3-bis-(3-octyloxyphenyl)quinoxaline-5,8-diyl-*alt*-thiophene-2,5-diyl](TQ1):[6,6]-phenyl-C 71 -butyric acid methyl ester (PC 71 BM), a noticeable power conversion efficiency of 6.42% with a high fill factor of 0.70 were obtained. These devices showed better long-term stability under ambient conditions than devices with common poly(3,4-ethylenedioxythiophene):poly-(styrene-sulfonate) (PEDOT:PSS) HTLs.

The factors affecting the adsorption performance of dyes on these materials include not only specific surface area, pore structure and distribution, but also the surface charges, and surface defects. To further improve the properties of solar cells, the relationship between physicochemical characteristics and solution technology should be established.

7. Conclusions and Outlook

This review article highlights the fundamentals and applications of solution combustion for the preparation of energy materials, including binary compounds, complex ternary and quaternary oxides, and nanocomposites. In many cases, solution combustion synthesis opens new opportunities for the synthesis of novel structures, such as surface oxygen vacancies, in situ heterojunctions. Furthermore, the application of the materials prepared via SCS in energy storage and conversion is also reviewed, such as lithium-ion batteries, supercapacitors, artificial photosynthesis, fuel cells, and photovoltaic solar cells. Although some outstanding advances have been made in the fabrication of complex nanomaterials with special structures and high performance, development of novel combustion synthesis techniques and engineering of surface oxygen vacancies, many challenging topics require further studies.

From the viewpoint of fundamental understanding of combustion science and technology, the correlations between the morphology, structure and fuel types, and heating rate are still not well established. Basically, the type of the starting materials, the fuel-oxidizer ratio, and the water amount in solution would affect thermodynamic variables including enthalpy, adiabatic flame temperature and the total amount of decomposed gas, which are related to the powder characteristics, such as crystal structure and surface area. In general, a good combustion synthesis does not proceed violently, would produce non-toxic gases and possess excellent complexing between metal salts and fuels. For example, when the solution is heated, water should be evaporated, which affects the stability of metal ions in the solution. Hence, the coordination ability of fuel, the type of metal salts, and the heating rate are key factors for designing objective materials. Furthermore, the type and amount of fuels and metal salts decide combustion temperature and the amount of released gases. The basic understanding of the raw materials should be improved. Moreover, surface oxygen defects can be easily created during solution combustion synthesis.

From the viewpoint of applications, the relationship between the performance and composition, structure of materials requires further studies. The design of materials with desired properties is still a great challenge. Especially, the regular porous materials or films with special properties should be exploited by solution combustion synthesis combined with template-assisted methods.

From the viewpoint of industrial production, the design and development of large-scale combustion reactors is necessary. The scale-up reactors should have the devices for introducing and emitting gas, collecting nanopowders, and basically, heating rate can be controlled.

This review focuses on the synthesis and applications of inorganic oxides and shows the progress and development trends in SCS to stimulate further efforts in the design and fabrication of new materials, and in studying the correlation between performance and properties of these materials.

Acknowledgements

This work was financially supported by the National Natural Science Foundation of China (No. 21376061, 21076060), the Program for New Century Excellent Talents in University (No. NCET-12-0686), Natural Science Foundation for Distinguished Young Scholar of Hebei Province (B2015208010), Scientific Research Foundation for High-Level Talent in University of Hebei Province (GCC2014057), and by the Australian Research Council (ARC) through the Discovery Project program (DP140104062, DP130104459). F. T. Li thanks the fund from China Scholarship Council.

Notes and references

[§]*The two authors have the equal contributions*

[a]*College of Science, Hebei University of Science and Technology, Shijiazhuang 050018*

[b]*School of Chemical Engineering, University of Adelaide, Adelaide, SA 5005, Australia. E-mail: s.qiao@adelaide.edu.au*

[c]*Department of Chemistry and Biochemistry, Kent State University, Kent, OH 44240, USA.*

1 J. A. Rodríguez, M. Fernández-García, Synthesis, properties, and applications of oxide nanomaterials, JohnWiley & Sons, Inc., Hoboken, New Jersey, 2007.
2 T. Guo, M. S. Yao, Y. H. Lin and C. W. Nan, *CrystEngComm*, 2015, **17**, 3551.
3 D. Bekermann, D. Barreca, A. Gasparotto and C. Maccato, *CrystEngComm*, 2012, **14**, 6347.
4 A. G. Merzhanov, *Ceram. Int*., 1995, **21**, 371.
5 S. L. Gonzalez-Cortes and F. E. Imbert, *Appl. Catal. A,* 2013, **452**, 117.
6 A. G. Merzhanov, *J. Mater. Chem.*, 2004, **14**, 1779.
7 X. T. Su, Q. Z. Yan and C. C. Ge, *Prog. Chem*., 2005, **17**, 430.
8 J. J. Kingsley and K. C. Patil, *Mater. Lett*., 1988, **6**, 427.
9 K. Rajeshwar and N. R. de Tacconi, *Chem. Soc. Rev.*, 2009, **38**, 1984.
10 J. S. Zhang, Q. J. Guo, Y. Z Liu and Y. Cheng, *Ind. Eng. Chem. Res*., 2012, **51**, 12773.
11 M. G. Kim, M. G. Kanatzidis, A. Facchetti1 and T. J. Marks. *Nat. Mater*., 2011, **10**, 382.
12 Y. Ren, Z. Ma and P. G. Bruce, *Chem. Soc. Rev*., 2012, **41**, 4909.
13 Y. Li , Z. Y. Fu and B. L. Su, *Adv. Funct. Mater.*, 2012, **22**, 4634.
14 N. Brun, L. Edembe, S. Gounel, N. Mano and M. M. Titirici, *ChemSusChem*, 2013, **6**, 701.
15 A. Kloke, C. Kohler, R. Gerwig, R. Zengerle and S. Kerzenmacher, *Adv. Mater*., 2012, **24**, 2916.
16 Z. J. Fan, J. Yan, G. Q. Ning, T. Wei, L. J. Zhi and F. Wei, *Carbon*, 2013, **60**, 558.
17 F. B. Li, X. P. Yao, Z. G. Wang, W. H. Xing, W. Q. Jin, J. Huang and Y. Wang, *Nano Lett*., 2012, **12**, 5033.

18 N. R. de Tacconi, H. K. Timmaji, W. Chanmanee, M. N. Huda, P. Sarker, C. Janaky and K. Rajeshwar, *ChemPhysChem*, 2012, **13**, 2945.

19 M. Lackner. Combustion Synthesis: Novel Routes to Novel Materials. Bentham science pubisher, 2010.

20 F. T. Li, Y. Liu, Z. M. Sun, R. H. Liu, L. J. Chen and D. S. Zhao, *Catal. Sci. Technol.*, 2012, **2**, 1455.

21 F. T. Li, Q. Wang, X. J. Wang, B. Li, Y. J. Hao, R. H. Liu and D. S. Zhao, *Appl. Catal. B,* 2014, **150**, 574.

22 J. C. Toniolo, A. S. Takimi and C. P. Bergmann, *Mater. Res. Bull*., 2010, **45**, 672.

23 Z. P. Yang, X. Li, Y. Yang and X. M. Li, *J. Lumin*., 2007, **122**, 707.

24 A. K. Deb, P. Chatterjee and S. P. S. Gupta, *Mater. Sci. Eng. A,* 2007, **59**, 124.

25 V. D. Zhuravlev, V. G. Bamburov, A. R. Beketov, L. A. Perelyaeva, I. V. Baklanova, O. V. Sivtsova, V. G. Vasilev, E. V. Vladimirova, V. G. Shevchenko and I. G. Grigorov, *Ceram. Int*., 2013, **39**, 1379.

26 P. Erri, P. Pranda and A. Varma, *Ind. Eng. Chem. Res*., 2004, **43**, 3092.

27 J. Toniolo, A. S. Takimi, M. J. Andrade, R. Bonadiman and C. P. Bergmann, *J. Mater. Sci*., 2007, **42**, 4785.

28 K. Deshpande, A. Mukasyan and A. Varma, *Chem. Mater*., 2004, **16**, 4896.

29 S. R. Jain, K. C. Adiga and V. R. P. Verneker, *Combus. Flame,* 1981, **40**, 71.

30 A. Kumar, E. E. Wolf and A. S. Mukasyan, *AIChE J*., 2011, **57**, 2207.

31 J. Bai, J. Liu, C. Li, G. Li and Q. Du, *Adv. Powder Technol*., 2011, **22**, 72.

32 M. M. A. Sekar and K. C. Patil, *Mat. Res. Bull.*, 1993, **28**, 485.

33 G. Sivalingam, K. Nagaveni, M. S. Hegde and G. Madras, *Appl. Catal. B*, 2003, **45**, 23.

34 A. Deshpande, G. Madras and N. M. Gupta, *Mater. Chem. Phys*., 2011, **126**, 546.

35 G. P. Nagabhushana, S. Ashoka, P. Chithaiah and G. T. Chandrappa, *Mater. Lett*., 2013, **91**, 272.

36 K. Suresh and K. C. Patil, *J. Mater. Sci. Lett*., 1993, **12**, 572.

37 A. S. Mukasyan and P. Dinka, *Int. J. Self Propag. High Temp. Synth*., 2007, **16**, 23.

38 K. Deshpande, M. Nersesyan, A. Mukasyan and A. Varma, *Ind. Eng. Chem. Res*., 2005, **44**, 6196.

39 R. Ianos, A. Taculescu, C. Pacurariu and I. Lazau, *J. Am. Ceram. Soc*., 2012, **95**, 2236.

40 Z. Abbasi, M. Haghighi, E. Fatehifar and S. Saedy, *J. Hazard. Mater.*, 2011, **186**, 1445.

41 M. Shekhar, J. Wang, W. S. Lee, W. D. Williams, S. M. Kim, E. A. Stach, J. T. Miller, W. N. Delgass and F. H. Ribeiro, *J. Am. Chem. Soc.,* 2012, **134**, 4700.

42 Y. K. Hong, D. W. Lee, H. J. Eom and K. Y. Lee, *Appl. Catal. B,* 2014, **150**, 438.

43 F. T. Li, Y. Zhao, Y. J. Hao, X. J. Wang, R. H. Liu, D. S. Zhao and D. M. Chen, *J. Hazard. Mater.*, 2012, **239**, 118.

44 F. T. Li, Y. Zhao, Y. Liu, Y. J. Hao, R. H. Liu and D. S. Zhao, *Chem. Eng. J*., 2011, **173**, 750.

45 W. Morales, M. Cason, O. Aina, N. R. de Tacconi and K. Rajeshwar, *J. Am. Ceram. Soc*., 2008, **130**, 6318.

46 A. Gupta, P. Ifeacho, C. Schulz and H. Wiggers, *P. Combust. Inst*., 2011, **33**, 1883.

47 M. Ahmad, Z. L. Hong, E. Ahmed, N. R. Khalid, A. Elhissi and W. Ahmad, *Ceram. Int*., 2013, **39**, 3007.

48 R. Nagaraja, C. R. Girija, B. M. Nagabhushana, N. Donappa and K. M. Sastry, *Asian J. Chem*., 2011, **23**, 5040.

49 L. H. Ai and J. Jiang, *Powder Technol*., 2009, **195**, 11.

50 P. Sahoo, H. Djieutedjeu and P. F. P. Poudeu, *J. Mater. Chem. A*, 2013, **1**, 15022.

51 T. L. Pfeil, T. L. Pourpoint and L. J. Groven, *Int. J. Hydrogen Energ*., 2014, **39**, 2149.

52 L. B. Fraigi, D. G. Lamas and N. E. W. de Reca, *Mater. Lett*., 2001, **47**, 262.

53 P. A. Deshpande, S. Polisetti and G. Madras, *Langmuir*, 2011, **27**, 3578.

54 G. P. Nagabhushana and G. T. Chandrappa, *J. Mater. Chem. A,* 2013, **1**, 11539.

55 S. K. Apte, S. D. Naik, R. S. Sonawane and B. B. Kale, *J. Am. Ceram. Soc*., 2007, **90**, 412.

56 A. Fujishima and K. Honda, *Nature*, 1972, **238**, 37.

57 T. L.Thompson and J. T. Yates, *Chem. Rev*., 2006, **106**, 4428.

58 A. B. Djurisic and Y. H. Leung, *Small*, 2006, **2**, 944.

59 X. B. Chen, S. H. Shen, L. J. Guo and S. S. Mao, *Chem. Rev.,* 2010**, 110**, 6503.

60 R. Asahi, T. Morikawa, T. Ohwaki, K. Aoki and Y. Taga, *Science,* 2001, **293**, 269.

61 Q. Zhang, D. Q. Lima, I. Lee, F. Zaera, M. F. Chi and Y. D. Yin, *Angew Chem. Int. Edit*., 2011, **50**, 7088.

62 J. Wang, D. N. Tafen, J. P. Lewis, Z. L. Hong, A. Manivannan, M. J. Zhi, M. Li and N. Q. Wu, *J. Am. Chem. Soc.,* 2009, **131**, 12290.

63 G. Liu, L. C. Yin, J. Q. Wang, P. Niu, C. Zhen, Y. P. Xie and H. M. Cheng, *Energy Environ. Sci*., 2012, **5**, 9603.

64 X. Yang, C. Cao, K. Hohn, L. Erickson, R. Maghirang, D. Hamal and K. Klabunde, *J. Catal.,* 2007, **252**, 296.

65 J. C. Yu, J. G. Yu, W. K. Ho, Z. T. Jiang and L. Z. Zhang, *Chem. Mater,* 2002, **14**, 3808.

66 X. X. Yang, C. D. Cao, L. Erickson, K. Hohn, R. Maghirang and K. Klabunde, *Appl. Catal. B,* 2009, **91**, 657.

67 J. Y Lee, J. Park and J. H. Cho, *Appl. Phys. Lett.*, 2005, **87**, 011904.

68 X. B. Chen and C. Burda, *J. Am. Chem. Soc.,* 2008, **130**, 5018.

69 J. B. Varley, A. Janotti and C. G. V. de Walle, *Adv. Mater.,* 2011, **23**, 2343.

70 S. U. M. Khan, M. Al-Shahry and W. B. Ingler, *Science,* 2002, **297**, 2243.

71 Q. Xiao and L. L. Ouyang, *Chem. Eng. J*., 2009, **148**, 248.

72 W. Ren, Z. Ai, F. Jia, L. Zhang, X. Fan and Z. Zou, *Appl. Catal. B,* 2007, **69**, 138.

73 K. Nagaveni, M. S. Hegde, N. Ravishankar, G. N. Subbanna and G. Madras, *Langmuir,* 2004**, 20**, 2900.

74 K. Nagaveni, G. Sivalingam, M. S. Hegde and G. Madras, *Appl. Catal. B,* 2004, **48**, 83.

75 A. D. Mani, B. R. Raju, N. Xanthopoulos, P. Ghosal, B. Sreedhar and C. Subrahmanyam, *Chem. Eng. J*., 2013, **228**, 545.

76 K. Sivaranjani and C. S. Gopinath, *J. Mater. Chem*., 2011, **21**, 2639.

77 M. Mapa and C. S. Gopinath, *Chem. Mater*., 2009, **21**, 351.

78 M. Mapa, K. S. Thushara, B. Saha, P. Chakraborty, C. M. Janet, R. P. Viswanath, C. M. Nair, K. V. G. K. Murty and C. S. Gopinath, *Chem. Mater*., 2009, **21**, 2973.

79 M. Mapa, K. Sivaranjani, D. S. Bhange, B. Saha, P. Chakraborty, A. K. Viswanath and C. S. Gopinath, *Chem. Mater*., 2010, **22**, 565.

80 G. S. Wu, J. L. Wen, S. Nigro and A. C. Chen, *Nanotechnology,* 2010, **21**, 085701.

81 S. Polisetti, P. A. Deshpande and G. Madras, *Ind. Eng. Chem. Res*., 2011, **50**, 12915.

82 P. Xu, T. Xu, J. Lu, S. M. Gao, N. S. Hosmane, B. B. Huang, Y. Dai and Y. B. Wang, *Energy Environ. Sci*., 2010, **3**, 1128.

83 K. Xie, N. Umezawa, N. Zhang, P. Reunchan, Y. J. Zhang and J. H. Ye, *Energy Environ. Sci.,* 2011, **4**, 4211.

84 G. M. Wang, Y. C. Ling, H. Y. Wang, X. Y. Yang, C. C. Wang, J. Z. Zhang and Y. Li, *Energy Environ. Sci*., 2012, **5**, 6180.

85 H. Li, S. Yin, Y. H. Wang, T. Sekino, S. W. Lee and T. Sato, *J. Catal*., 2013, **297**, 65.

86 Y. H. Lv, C. S. Pan, X. G. Ma, R. L. Zong, X. J. Bai and Y. F. Zhu, *Appl. Catal. B,* 2013, **138–139**, 26.

87 M. Kong, Y. Z. Li, X. Chen, T. T. Tian, P. F. Fang, F. Zheng and X. J. Zhao, *J. Am. Chem. Soc.,* 2011, **133**, 16414.

88 Q. P. Wu and R. Krol, *J. Am. Chem. Soc*., 2012, **134**, 9369.

89 F. T. Li, Q. Wang, J. R. Ran, Y. J. Hao, X. J. Wang, D. S. Zhao and S. Z. Qiao, *Nanoscale*, 2015, **7**, 1116.

90 V. M. Sharma, D. Saha, G. Madras and T. N. G. Row, *RSC Adv.*, 2013, **3**, 18938.

91 F. Zuo, L. Wang, T. Wu, Z. Y. Zhang, D. Borchardt and P. Y. Feng, *J. Am. Chem. Soc*., 2010, **132**, 11856.

92 F. Zuo, L. Wang and P. Y. Feng, *Int. J. Hydrogen Energy,* 2014, **39**, 711.

93 Y. H. Ni, Y. Zhu and X. Ma*, Dalton Trans*., 2011, **40**, 3689.

94 B. Murugan and A. V. Ramaswamy, *J. Phys. Chem. C,* 2008, **112**, 20429.
95 B. Guan, H. Lin, L. Zhu, B. Tian and Z. Huang, *Chem. Eng. J.*, 2012, **181–182**, 307.
96 C. Q. Chen, Y. Yu, W. Li, C. Y. Cao, P. Li, Z. F. Dou and W. G. Song, *J. Mater. Chem.,* 2011, **21**, 12836.
97 S. Ekambaram, Y. Iikubo and A. Kudo, *J. Alloy. Compd*., 2007, **433**, 237.
98 M. Ahmad, E. Ahmed, Y. W. Zhang, N. R. Khalid, J. F. Xu, M. Ullah and Z. L. Hong, *Curr. Appl. Phys*., 2013, **13**, 697.
99 S. S. Thind, G. S. Wu and A. C. Chen, *Appl. Catal. B,* 2012, **111**, 38.
100 J. Nuneza, V. A. de la Pena O'Shea, P. Jana, J. M. Coronado and D. P. Serrano, *Catal. Today,* 2013, **209**, 21.
101 G. S. Wu, J. L. Wen, J. P. Wang, D. F. Thomas and A. C. Chen, *Mater. Lett*., 2010, **64**, 1728.
102 M. A. Pena and J. L. G. Fierro, *Chem. Rev*., 2001, **101**, 1981.
103 S. S. Manoharan and K. C. Patil, *J. Solid State Chem.,* 1993, **102**, 267.
104 F. Stevens, R. Cloots, D. Poelman, B. Vertruyen and C. Henrist, *Mater. Lett.,* 2014, **114**, 136.
105 X. Chen, S. J. Liang, J. H. Bi, J. Gao and L. Wu, *Chinese J. Inorg. Chem*., 2009, **25**, 1922.
106 Q. Y. Chen, X. Gu, Y. H. Wang and D. W. Jing, *Sci. Adv. Mater*., 2013, **5**, 1117.
107 L. Wu, J. C. Yu, L. Z. Zhang, X. C. Wang and S. K. Li, *J. Solid State Chem*., 2004, **177**, 3666.
108 T. H. Shin, S. Ida and T. Ishihara, *J. Am. Chem. Soc*., 2011, **133**, 19399.
109 F. T. Li, Y. Liu, R. H. Liu, Z. M. Sun, D. S. Zhao and C. G. Kou, *Mater. Lett.,* 2010, **64**, 223.
110 K. M. Parida, K. H. Reddy, S. Martha, D. P. Das and N. Biswal, *Int. J. Hydrogen Energy,* 2010, **35**, 12161.
111 G. S. Gallego, N. M. Alzate and O. Arnache, *J. Alloy. Compd*., 2013, **549**, 163.
112 F. T. Li, Y. Liu, Z. M. Sun, R. H. Liu, C. G. Kou, Y. Zhao and D. S. Zhao, *Mater. Lett.*, 2011, **65**, 406.
113 R. R. Kondakindi, K. Karan and B. A. Peppley, *Ceram. Int.,* 2012, **38**, 449.
114 Z. X. Wei, Y. Wang, J. P. Liu, C. M. Xiao and W. W. Zeng, *Mater. Chem. Phys*., 2012, **136**, 755.
115 H. Xue, Z. H. Li, X. X. Wang and X. Z. Fu, *J. Phys. Chem. Solids,* 2007, **68**, 2326.
116 J. Yang, X. C. Li, J. Y. Zhou, Y. Tang, Y. M. Zhang and Y. W. Li, *J. Alloy. Compd*., 2011, **509**, 9271.
117 Y. Y. Li, S. S. Yao, W. Wen, L. H. Xue and Y. W. Yan, *J. Alloy. Compd*., 2010, **491**, 560.
118 Y. A. Chaudhari, A. Singh, C. M. Mahajan, P. P. Jagtap, E. M. Abuassaj, R. Chatterjee and S. T. Bendre, *J. Magn. Magn. Mater.*, 2013, **347**, 153.
119 J. M. Wu and W. Wen, *Environ. Sci. Technol*, 2010**, 44**, 9123.
120 D. Saha, G. Madras and T. N. G. Row, *Mater. Res. Bull.*, 2011, **46**, 1252.
121 R. Ianos, I. Lazau, C. Pacurariu and P. Barvinschi, *Mater. Res. Bull*., 2008, **43**, 3408.
122 H. Jeong and M. Kang, *Appl. Catal. B*, 2010, **95**, 446.
123 O. R. Evans, A. T. Bell and T. D. Tilley, *J. Catal*., 2004, **226**, 292.
124 W. C. Li, M. Comotti, A. H. Lu and F. Schuth, *Chem. Comm*., 2006, 1772.
125 A. Laobuthee, S. Wongkasemjit, E. Traversa and R. M. Laine, *J. Eur. Ceram. Soc*., 2000, **20**, 91.
126 A. Chartier, T. Yamamoto, K. Yasuda, C. Meis and S. Matsumur, *J. Nucl. Mater.*, 2008, **378**, 188.
127 M. Ishimaru, Y. Hirotsu, I. V. Afanasyev-Charkin and K. E. Sickafus, *J. Phys.: Condens. Matter*, 2002, **14**, 1237.
128 K. Suresh, N. R. S. Kumar and K. C. Patil, *Adv. Mater.*, 1991, **3**, 3.
129 T. Tangcharoen, A. Ruangphanit, W. Klysubun and W. Pecharapa, *J. Sol-Gel Sci. Technol.*, 2013, **66**, 387.
130 A. I. Borhan, P. Samoila, V. Hulea, A. R. Iordan and M. N. Palamaru, *J. Photochem. Photobio. A*, 2014, **279**, 17.
131 C. Choodamani, G. P. Nagabhushana, S. Ashoka, B. D. Prasad, B. Rudraswamy and G. T. Chandrappa, *J. Alloy. Compd*., 2013, **578**, 103.
132 P. S. Sathiskumar, C. R. Thomas and G. Madras, *Ind. Eng. Chem. Res*., 2012, **51**, 10108.
133 S. Mestre, M. D. Palacios and P. Agut, *J. Eur. Ceram. Soc*., 2012, **32**, 1995.
134 J. J. Ding, S. Sun, J. Bao, Z. L. Luo and C. Gao, *Catal. Lett*., 2009, **130**, 147.
135 T. W. Kim and K. S. Choi, *Science,* 2014*,* **343**, 990.
136 S. Tokunaga, H. Kato and A. Kudo, *Chem. Mater*., 2001, **13**, 4624.
137 G. P. Nagabhushana, G. Nagaraju and G. T. Chandrappa, *J. Mater. Chem. A,* 2013, **1**, 388.
138 B. Xie, H. Zhang, P. Cai, R. Qiu and Y. Xiong, *Chemosphere*, 2006, **63**, 956.
139 M. Kakihana, *J. Sol-Gel Sci. Technol.*, 1996, **6**, 7.
140 Z. J. Zhang, W. Z. Wang, M. Shang and W. Z. Yin, *Catal. Commun*., 2010, **11**, 982.
141 H. Q. Jiang, H. Endo, H. Natori, M. Nagai and K. Kobayashi, *J. Eur. Ceram. Soc*., 2008, **28**, 2955.
142 U. M. G. Perez, S. Sepulveda-Guzman, A. Martinez-de la Cruz and U. O. Mendez, *J. Mol. Catal. A*, 2011, **335**, 169.
143 M. R. da Silva, L. H. Dall'Antonia, L. V. A. Scalvi, D. I. dos Santos, L. O. Ruggiero and A. Urbano, *J. Solid State Electrochem*., 2012, **16**, 3267.
144 M. R. Silva, A. C. Lucilha, R. Afonso, L. H. Dall'Antonia and L. V. A. Scalvi, *Ionics*, 2014, **20**, 105.
145 J. G. Qu, N. N. Li, B. J. Liu and J. X. He, *Mat. Sci. Semicon. Proc*., 2013, **16**, 99.
146 D. Baykan and N. A. Oztas, *Mater. Res. Bull*., 2012, **47**, 4013.
147 T. T. Dong, Z. H. Li, Z. X. Ding, L. Wu, X. X. Wang and X. Z. Fu, *Mater. Res. Bull.,* 2008, **43**, 1694.
148 P. A. Deshpande and G. Madras, *Chem. Eng. J*., 2010, **158**, 571.
149 Z. J. Zhang, W. Z. Wang, M. Shang and W. Z. Yin, *J. Hazard. Mater*., 2010, **177**, 1013.
150 D. Saha, G. Madras and T. N. G. Row, *Dalton Trans*., 2012, **41**, 9598.
151 O. Subohi, G. S. Kumar, M. M. Malik and R. Kurchania, *Physica B,* 2012, **407**, 3813.
152 S. M. Yin, W. X. Zhang, L. H. Xue and Y. W. Yan, *J. Mater. Sci.,* 2013, **48**, 1533.
153 A. Choudhary, B. S. Sahu, R. Mazumder, S. Bhattacharyya and P. Chaudhuri, *J. Alloy. Compd.*, 2014, **590**, 440.
154 P. Manikandan, M. V. Ananth, T. P. Kumar, M. Raju, P. Periasamy and K. Manimaran, *J. Power Sources*, 2011, **196**, 10148.
155 S. S. M. Bhat and N. G. Sundaram, *RSC Adv*., 2013, **3**, 14371.
156 S. Rodrigues, N. Munichandraiah and A. K. Shukla, *J. Power Sources*, 2001, **102**, 322.
157 C. Y. Zhu, A. Nobuta, Y. W. Ju, T. Ishihara and T. Akiyama, *Int. J. Hydrogen Energ.*, 2013, **38**, 13419.
158 W. D. Wang, F. Q. Huang, C. M. Liu, X. P. Lin and J. L. Shi, *Mater. Sci. Eng. B*, 2007, **139**, 74.
159 Y. Q. Qu and X. F. Duan, *Chem. Soc. Rev.*, 2013, **42**, 2568.
160 Y. J. Wang, Q. F. Wang, X. Y. Zhan, F. M. Wang, M. Safdar and J. He, *Nanoscale*, 2013, **5**, 8326.
161 W. L. Yang, L. Zhang, Y. Hu, Y. J. Zhong, H. B. Wu and X. W. Lou, *Angew. Chem. Int. Ed*., 2012, **51**, 11501.
162 Y. Zhao, C. Z. Li, X. H. Liu, F. Gu, H. L. Du and L. Y. Shi, *Appl. Catal. B*, 2008, **79**, 208.
163 H. Q. Jiang, H. Endo, H. Natori, M. Nagai and K. Kobayashi, *Mater. Res. Bull*., 2009, **44**, 700.
164 T. G. Li, S. W. Liu, H. P. Zhang, E. H. Wang, L. J. Song and P. Wang, *J. Mater. Sci.*, 2011, **46**, 2882.
165 X. P. Pu, D. F. Zhang, Y. Y. Gao, X. Shao, G. Q, Ding, S. S. Li and S. P, Zhao, *J. Alloy. Compd*., 2013, **551**, 382.
166 Y. Y. Gao, X. P. Pu, D. F. Zhang, G. Q. Ding, X. Shao and J. Ma, *Carbon*, 2012, **50**, 4093.
167 D. F. Zhang, X. P. Pu., Y. Y. Gao, C. H. Su, H. Li, H. Y. Li and W. X. Hang, *Mater. Lett*., 2013, **113**, 179.
168 D. F. Zhang, Q. Ding, X. P. Pu, C. H. Su, X. Shao, G. Q. Ding, Z. G. Zhang and Q. N. Fang, *Funct. Mater. Lett*., 2014, **7**, 1350065.
169 P. Dinka and A. S. Mukasyan, *J. Phys. Chem. B*, 2005, **109**, 21627.

170 B. M. Reddy, G. K. Reddy, K. N. Rao, I. Ganesh and J. M. F. Ferreira, *J. Mater. Sci*., 2009, **44**, 4874.

171 Y. J. Hao, F. T. Li, F. Chen, M. J. Chai, R. H. Liu and X. J. Wang, *Mater. Lett*., 2014, **124**, 1.

172 A. Nashim and K. M. Parida, *Chem. Eng. J*., 2013, **215**, 608.

173 K. M. Parida, A. Nashim and S. K. Mahanta, *Dalton Trans*., 2011, **40**, 12839.

174 G. K. Pradhan, S. Martha and K. M. Parida, *ACS Appl. Mater. Interfaces*, 2012, **4**, 707.

175 H. Q. Jiang, M. Nagai and K. Kobayashi, *J. Alloy. Compd*., 2009, **479**, 821.

176 N. G. Moustakas, A. G. Kontos, V. Likodimos, F. Katsaros, N. Boukos, D. Tsoutsou, A. Dimoulas, G. E. Romanos, D. D. Dionysiou and P. Falaras, *Appl. Catal. B*, 2013, **130**, 14.

177 A. S. Prakash, C. Shivakumara and M. S. Hegde, *Mater. Sci. Eng. B*, 2007, **139**, 55.

178 S. T. Aruna, N. S. Kini and K. S. Rajam, *Mater. Res. Bull*., 2009, **44**, 728.

179 S. Sakurai, A. Namai, K. Hashimoto and S. I. Ohkoshi, *J. Am. Chem. Soc*., 2009, **131**, 18299.

180 K. L. Zhang, C. M. Liu, F. Q. Huang, C. Zheng and W. D. Wang, *Appl. Catal. B*, 2006, **68**, 125.

181 U. Eggenweiler, E. Keller and V. KraEmer, *Acta Crystallogr. B*, 2000, **56**, 431.

182 K. Tahmasebi and M. H. Paydar, *Mater. Chem. Phys*., 2008, **109**, 156.

183 K. V. Manukyan, A. Cross, S. Roslyakov, S. Rouvimov, A. S. Rogachev, E. E. Wolf and A. S. Mukasyan, *J. Phys. Chem. C*, 2013, **117**, 24417.

184 K. R. Priolkar, P. Bera, P. R. Sarode, M. S. Hegde, S. Emura, R. Kumashiro and N. P. Lalla|, *Chem. Mater.*, 2002, **14**, 2120.

185 S. Sontakke, J. Modak and G. Madras, *Chem. Eng. J.*, 2010, **165**, 225.

186 P. Bera, K. C. Patil, V. Jayaram, M. S. Hegde and G. N. Subbanna, *J. Mater. Chem.*, 1999, **9**, 1801.

187 S. Sontakke, C. Mohan, J. Modak and G. Madras, *Chem. Eng. J*., 2012, **189-190**, 101.

188 Y. Cai, H. Q. Fan, M. M. Xu and Q. Li, *Colloid. Surface A*, 2013, **436**, 787.

189 S. A. Ansari, M. M. Khan, J. Lee and M. H. Cho, *J. Ind. Eng. Chem*., 2014, **20**, 1602.

190 S. Colussi, A. Gayen, J. Llorca, C. de Leitenburg, G. Dolcetti and A. Trovarelli, *Ind. Eng. Chem. Res*., 2012, **51**, 7510.

191 P. Bera, K. C. Patil, V. Jayaram, G. N. Subbanna and M. S. Hegde, *J. Catal*., 2000, **196**, 293.

192 Y. J. Hao, F. T. Li, S. S. Wang, M. J. Chai, R. H. Liu and X. J. Wang, *Mater. Sci. Eng. B*, 2014, **186**, 41.

193 A. M. Zhao, W. Y. Ying, H. T. Zhang, H. F. Ma and D. Y. Fang, *Catal. Commun*., 2012, **17**, 34.

194 H. Nasiri, J. Vahdati Khaki and S. M. Zebarjad, *J. Alloy. Compd*., 2011, **509**, 5305.

195 L. H. Reddy, G. K. Reddy, D. Devaiah and B. M. Reddy, *Appl. Catal. A,* 2012, **445–446**, 297.

196 J. B. Goodenough and K. S. Park, *J. Am. Chem. Soc*., 2013, **135**, 1167.

197 X. Su, Q. L. Wu, J. C. Li, X. C. Xiao, A. Lott, W. Q. Lu, B. W. Sheldon and J. Wu, *Adv. Energy Mater.,* 2014, **4**, 1300882.

198 Z. Y. Weng, H. Guo, X. M. Liu, S. L. Wu, K. W. K. Yeung and P. K. Chu, *RSC Adv*., 2013, **3**, 24758.

199 X. H. Rui, Q. Y. Yan, M. Skyllas-Kazacose, T. M. Lim, *J. Power Sources,* 2014, **258**, 19.

200 C. Julien, M. A. Camacho-Lopez, T. Mohan, S. Chitra, P. Kalyani and S. Gopukumar, *Solid State Ionics*, 2000, **135**, 241.

201 P. Kalyani, N. Kalaiselvi and N. Muniyandi, *J. Power Sources*, 2002, **111**, 232.

202 P. Suresh, S. Rodrigues, A. K. Shukla, S. A. Shivashankar and N. Munichandraiah, *J. Power Sources*, 2002, **112**, 665.

203 P. Periasamy, H. S. Kim, S. H. Na, S. I. Moon and J. C. Lee, *J. Power Sources*, 2004, **132**, 213.

204 Y. Bentaleb, I. Saadoune, K. Maher, L. Saadi, K. Fujimoto and S. Ito, *J. Power Sources*, 2010, **195**, 1510.

205 Y. S. Hong, Y. J. Park, K. S. Ryu, S. H. Chang and Y. J. Shin, *J. Power Sources*, 2005, **147**, 214.

206 D. C. Li, T. Muta and H. Noguchi, *J. Power Sources*, 2004, **135**, 262.

207 T. Ohzuku and Y. Makimura, *Chem. Lett*., 2001, **30**, 744.

208 Y. J. Park, Y. S. Hong, X. Wu, K. S. Ryu and S. H. Chang, *J. Power Sources*, 2004, **129**, 288.

209 S. K. Martha, H. Sclar, Z. S. Framowitz, D. Kovacheva, N. Saliyski, Y. Gofer, P. Sharon, E. Golik, B. Markovsky and D. Aurbach, *J. Power Sources*, 2009, **189**, 248.

210 C. Z. Lu and G. T. K. Fey, *J. Phys. Chem. Solids*, 2006, **67**, 756.

211 K. R. Ragavendran, L. Lu, K. Barner and A. K. Arof, *J. Phys. Chem. C*, 2013, **117**, 23547.

212 K. Ragavendran, D. Sherwood, D. Vasudevan and B. Emmanuel, *Physica B*, 2009, **404**, 2166.

213 M. Jayalakshmi, M. Mohan Rao and F. Scholz, *Langmuir*, 2003, **19**, 8403.

214 S. Y. Chew, T. J. Patey, O. Waser, S. H. Ng, R. Büchel, A. Tricoli, F. Krumeich, J. Wang, H. K. Liu, S. E. Pratsinis and P. Novak, *J. Power Sources*, 2009, **189**, 449.

215 A. K. Padhi, K. S. Nanjundaswamy and J. B. Goodenough, *J. Electrochem. Soc.*, 1997, **144**, 1188.

216 B. T. Zhao, X. Yu, R. Cai, R. Ran, H. T. Wang and Z. P. Shao, *J. Mater. Chem*., 2012, **22**, 2900.

217 L. Vijayan, R. Cheruku and G. Govindaraj, *Mater. Res. Bull*., 2014, **50**, 341.

218 R. W. Mo, Z. Y. Lei, K. N. Sun and D. Rooney, *Adv. Mater*., 2014, **26**, 2084.

219 Z. Y. Sun, X. Huang, M. Muhler, W. G. Schuhmann and E. Ventosa, *Chem. Commun*., 2014, **50**, 5506.

220 R. Yi, F. Dai, M. L. Gordin, S. R. Chen and D. H. Wang, *Adv. Energy Mater.* 2013, **3**, 295.

221 Y. H. Xu, Y. J. Zhu, Y. H. Liu and C. S. Wang, *Adv. Energy Mater.*, 2013, **3**, 128.

222 F. Han, D. Li, W. C. Li, C. Lei, Q. Sun and A. H. Lu, *Adv. Funct. Mater.*, 2013, **23**, 1692.

223 B. H. Li, C. P. Han, Y. B. He, C. Yang, H. D. Du, Q. H. Yang and F. Y. Kang, *Energy Environ. Sci*., 2012, **5**, 9595.

224 K. Nathiya, D. Bhuvaneswari, Gangulibabu, D. Nirmala and N. Kalaiselvi, *RSC Adv*., 2012, **2**, 6885.

225 P. Poizot, S. Laruelle, S. Grugeon, L. Dupont and J. M. Tarascon, *Nature*, 2000, **407**, 496.

226 J. Cabana, L. Monconduit, D. Larcher and M. R. Palacín, *Adv. Mater*., 2010, **22**, E170.

227 W. Wen, J. M. Wu and J. P. Tu, *J. Alloy. Compd*., 2012, **513**, 592.

228 X. Zhao, D. Xia and K. Zheng, *J. Alloy. Compd*., 2012, **513**, 460.

229 L. Zhang, H. B. Wu and X. W. Lou, *Adv. Energy Mater.*, 2014, **4**, 1300958.

230 J. Lin, A. R. O. Raji, K. W. Nan, Z. W. Peng, Z. Yan, E. L. G. Samuel, D. Natelson and J. M. Tour, *Adv. Funct. Mater.*, 2014, **24**, 2044.

231 Z. Y. Wang, L. Zhou and X. W. Lou, *Adv. Mater.*, 2012, **24**, 1093.

232 J. M. Haag, G. Pattanaik and M. F. Durstock, *Adv. Mater.*, 2013, **25**, 3238.

233 W. Wen and J. M. Wu, *ACS Appl. Mater. Interfaces*, 2011, **3**, 4112.

234 P. Gomathisankar, K. Hachisuka, H. Katsumata, T. Suzuki, K. Funasaka and S. Kaneko, *ACS Sustainable Chem. Eng*., 2013, **1**, 982.

235 P. Y. Li, J. C. Deng, Y. Li, W. Liang, K. Wang, L. T. Kang, S. Z. Zeng, S. H. Yin, Z. G. Zhao, X. G. Liu, Y. Z. Yang and F. Gao, *J. Alloy. Compd*., 2014, **590**, 318.

236 J. Chen, L. N. Xu, W. Y. Li and X. L. Gou, *Adv. Mater*., 2005, **17**, 582.

237 A. S. Prakash, P. Manikandan, K. Ramesha, M. Sathiya,J-M. Tarascon and A. K. Shukla, *Chem. Mater*., 2010, **22**, 2857.

238 T. Yuan, R. Cai, K. Wang, R. Ran, S. M. Liu and Z. P. Shao, *Ceram. Int*., 2009, **35**, 1757.

239 X. Li, H. C. Lin, W. J. Cui, Q. Xiao and J. B. Zhao, *ACS Appl. Mater. Interfaces*, 2014, **6**, 7895.

240 X. Li, Q. Xiao, B. Liu, H. C. Lin and J. B. Zhao, *J. Power Sources*, 2015, **273**, 128.

241 A. Kraytsberg and Y. Ein-Eli, *Adv. Energy Mater.*, 2012, **2**, 922.

242 A. Vu, Y. Q. Qian and A. Stein, *Adv. Energy Mater.*, 2012, **2**, 1056.
243 L. L. Zhang and X. S. Zhao, *Chem. Soc. Rev.*, 2009, **38**, 2520.
244 W. F. Wei, X. W. Cui, W. X. Chen and D. G. Ivey, *Chem. Soc. Rev.*, 2011, **40**, 1697.
245 S. Chen, W. Xing, J. J. Duan, X. J. Hu and S. Z. Qiao, *J. Mater. Chem. A*, 2013, **1**, 2941.
246 J. Yan , Q. Wang , T. Wei and Z. J. Fan, *Adv. Energy Mater.*, 2014, **4**, 1300816.
247 A. Pendashteh, M. S. Rahmanifar, R. B. Kaner and M. F. Mousavi, *Chem. Commun.*, 2014, **50**, 1972.
248 Y. Sharma, N. Sharma, G. V. S. Rao and B. V. R. Chowdari, *J. Power Sources*, 2007, **173**, 495.
249 M. V. Reddy, C. Yu, F. Jiahuan, K. P. Loh and B. V. R. Chowdari, *RSC Adv.*, 2012, **2**, 9619.
250 W. Xiao, J. S. Chen, C. M. Li, R. Xu and X. W. Lou, *Chem. Mater.*, 2010, **22**, 746.
251 J. Haetge, I. Djerdj and T. Brezesinski, *Chem. Commun.*, 2012, **48**, 6726.
252 L. Q. Mai, F. Yang, Y. L. Zhao, X. Xu, L. Xu and Y. Z. Luo, *Nat. Commun.*, 2011, **2**, 381.
253 D. P. Cai, D. D. Wang, B. Liu, Y. R. Wang, Y. Liu, L. L. Wang, H. Li, H. Huang, Q. H. Li and T. H. Wang, *ACS Appl. Mater. Inter.*, 2013, **5**,12905.
254 J. Chang, M. Jin, F. Yao, T. H. Kim, V. T. Le, H. Yue, F. Gunes, B. Li, A. Ghosh, S. Xie and Y. H. Lee, *Adv. Funct. Mater.*, 2013, **23**, 5074.
255 B. Senthilkumar, K. Vijaya Sankar, R. Kalai Selvan, M. Danielle and M. Manickam, *RSC Adv.*, 2013, **3**, 352.
256 B. Senthilkumar, D. Meyrick, Y. S. Lee and R. K. Selvan, *RSC Adv.*, 2013, **3**, 16542.
257 H. G. Jung, N. Venugopal, B. Scrosati and Y. K. Sun, *J. Power Sources*, 2013, **221**, 266.
258 H. S. Choi, J. H. Im, T. Kim, J. H. Park and C. R. Park, *J. Mater. Chem.*, 2012, **22**, 16986.
259 B. Wang, T. R. Kang, N. Xia, F. Y. Wen and L. M. Chen, *Ionics*, 2013, **19**, 1527.
260 H. U. Kim, Y. K. Sun, K. H. Shin and C. S. Jin, *Phys. Scr.*, 2010, ***T139***, 014053.
261 M. Jayalakshmi, M. Palaniappa and K. Balasubramanian, *Int. J. Electrochem. Sci.*, 2008, **3**, 96.
262 M. Jayalakshmi and K. Balasubramanian, *Int. J. Electrochem. Sci.*, 2009, **4**, 878.
263 M. R. Gao, Y. F. Xu, J. Jiang and S. H. Yu, *Chem. Soc. Rev.*, 2013, **42**, 2986.
264 S. Berardi, S. Drouet, L. Francas, C. Gimbert-Surinach, M. Guttentag, C. Richmond, T. Stoll and A. Llobet, *Chem. Soc. Rev.*, 2014, **43**, 7501.
265 M. Cargnello, A. Gasparotto, V. Gombac, T. Montini, D. Barreca and P. Fornasiero, *Eur. J. Inorg. Chem.*, 2011, 4309.
266 D. Barreca, G. Carraro, V. Gombac, A. Gasparotto, C. Maccato, P. Fornasiero and E. Tondello, *Adv. Funct. Mater.*, 2011, **21**, 2611.
267 S. Kaneco, T. Miwa, K. Hachisuka, H. Katsumata, T. Suzuki, S. C. Verma and K. Sugihara, Nanocatalysis for Fuels and Chemicals, Chapter 2, ACS Symposium Series, 2012, Vol. 1092.
268 M. E. A. Warwick, K. Kaunisto, D. Barreca, G. Carraro, A. Gasparotto, C. Maccato, E. Bontempi, C. Sada, T. P. Ruoko, S. Turner and G. V. Tendeloo, *ACS Appl. Mater. Interfaces*, 2015, **7**, 8667.
269 L. J. Groven, T. L. Pfeil and T. L. Pourpoint, *Int. J. Hydrogen Energ.*, 2013, **38**, 6377.
270 X. M. Ge, S. H. Chan, Q. L. Liu and Q. Sun, *Adv. Energy Mater.*, 2012, **2**, 1156.
271 S. T. Aruna, M. Muthuraman and K. C. Patil, *J. Mater. Chem.*, 1997, **7**, 2499.
272 C. W. Sun and U. Stimming, *J. Power Sources*, 2007, **171**, 247.
273 M. Shishkin and T. Ziegler, *J. Phys. Chem. C*, 2010, **114**, 21411.
274 A. D. Lan and A. S. Mukasyan, *J. Phys. Chem. C*, 2007, **111**, 9573.
275 W. G. Zhao, S. L. An and L. Ma, *J. Am. Chem. Soc.*, 2011, **94**, 1496.
276 M. G. Bellino, D. G. Lamas and N. E. W. de Reca, *Adv. Mater.*, 2006, **18**, 3005.
277 M. Yan, T. Mori, J. Zou and J. Drennan, *J. Am. Chem. Soc.*, 2009, **92**, 2745.
278 N. Jaiswal, S. Upadhyay, D. Kumar and O. Parkash, *Int. J. Hydrogen Energ.*, 2014, **39**, 543.
279 B. S. Prakash, V. K. W. Grips and S. T. Aruna, *J. Power Sources*, 2012, **214**, 358.
280 G. Kim, N. Lee, K. B. Kim, B. K. Kim, H. Chang, S. J. Song and J. Y. Park, *Int. J. Hydrogen Energ.*, 2013, **38**, 1571.
281 J. Chen, F. Liang, L. Liu, S. P. Jiang and L. Jian, *Int. J. Hydrogen Energ.*, 2009, **34**, 6845.
282 C. Zhu, A. Nobuta, I. Nakatsugawa and T. Akiyama, *Int. J. Hydrogen Energ.*, 2013, **38**, 13238.
283 J. Roncali, *Adv. Energy Mater.*, 2011, **1**, 147.
284 G. Q. Zhang, S. Finefrock, D. X. Liang, G. G. Yadav, H. R. Yang, H. Y. Fang and Y. Wu, *Nanoscale*, 2011, **3**, 2430.
285 M. L. Brongersma, Y. Cui and S. H. Fan, *Nat. Mater.*, 2014, **13**, 451.
286 B. Oregan and M. Gratzel, *Nature*, 1991, **353**, 737.
287 S. L. Chung and C. M. Wang, *J. Mater. Sci. Technol.*, 2012, **28**, 713.
288 D. J. Lipomi, B. C. K. Tee, M. Vosgueritchian and Z. Bao, *Adv. Mater.*, 2011, **23**, 1771.
289 R. Zhu, A. Kumar and Y. Yang, *Adv. Mater.*, 2011, **23**, 4193.
290 C. Yao, X. J. Xu, J. S. Wang, L. L. Shi and L. D. Li, *ACS Appl. Mater. Interfaces*, 2013, **5**, 1100.
291 H. Ma, H. L. Yip, F. Huang and A. K. Y. Jen, *Adv. Funct. Mater.*, 2010, **20**, 1371 .
292 Y. Zhou, C. Fuentes-Hernandez, J. Shim, J. Meyer, A. J. Giordano, H. Li, P. Winget, T. Papadopoulos, H. Cheun, J. Kim, M. Fenoll, A. Dindar, W. Haske, E. Najafabadi, T. M. Khan, H. Sojoudi, S. Barlow, S. Graham, J. L. Bredas, S. R. Marder, A. Kahn and B. Kippelen, *Science*, 2012, **336**, 327.
293 Z. Tang, L. M. Andersson, Z. George, K. Vandewal, K. Tvingstedt, P. Heriksson, R. Kroon, M. R. Andersson and O. Inganas, *Adv. Mater.*, 2012, **24**, 554 .
294 S. Bai, M. T. Cao, Y. Z. Jin, X. L. Dai, X. Y. Liang, Z. Z. Ye, M. Li, J. P. Cheng, X. Z. Xiao, Z. W. Wu, Z. H. Xia, B. Q. Sun, E. G. Wang, Y. Q. Mo, F. Gao and F. L. Zhang, *Adv. Energy Mater.*, 2014, **4**, 1301460.